Molecular Therapy
Original Article

Rescue of Hearing by Gene Delivery to Inner-Ear Hair Cells Using Exosome-Associated AAV

Bence György,[1,2,6] Cyrille Sage,[1,6] Artur A. Indzhykulian,[1] Deborah I. Scheffer,[1] Alain R. Brisson,[3] Sisareuth Tan,[3] Xudong Wu,[1] Adrienn Volak,[2] Dakai Mu,[2] Panos I. Tamvakologos,[1] Yaqiao Li,[1] Zachary Fitzpatrick,[2] Maria Ericsson,[4] Xandra O. Breakefield,[2,5] David P. Corey,[1,6] and Casey A. Maguire[2,6]

[1]Department of Neurobiology and Howard Hughes Medical Institute, Harvard Medical School, 220 Longwood Avenue, Boston, MA 02115, USA; [2]Department of Neurology, Massachusetts General Hospital and NeuroDiscovery Center, Harvard Medical School, Building 149, Charlestown, Boston, MA 02129, USA; [3]Molecular Imaging and NanoBioTechnology, UMR-5248-CBMN CNRS-University of Bordeaux-IPB, Allée Geoffroy Saint-Hilaire, F-33600 Pessac, France; [4]Department of Cell Biology, Harvard Medical School, 220 Longwood Avenue, Boston, MA 02115, USA; [5]Program in Neuroscience, Harvard Medical School, Building 149, Charlestown, Boston, MA 02129, USA

Adeno-associated virus (AAV) is a safe and effective vector for gene therapy for retinal disorders. Gene therapy for hearing disorders is not as advanced, in part because gene delivery to sensory hair cells of the inner ear is inefficient. Although AAV transduces the inner hair cells of the mouse cochlea, outer hair cells remain refractory to transduction. Here, we demonstrate that a vector, exosome-associated AAV (exo-AAV), is a potent carrier of transgenes to all inner ear hair cells. Exo-AAV1-GFP is more efficient than conventional AAV1-GFP, both in mouse cochlear explants in vitro and with direct cochlear injection in vivo. Exo-AAV shows no toxicity in vivo, as assayed by tests of auditory and vestibular function. Finally, exo-AAV1 gene therapy partially rescues hearing in a mouse model of hereditary deafness (lipoma HMGIC fusion partner-like 5/tetraspan membrane protein of hair cell stereocilia [*Lhfpl5/Tmhs*$^{-/-}$]). Exo-AAV is a powerful gene delivery system for hair cell research and may be useful for gene therapy for deafness.

INTRODUCTION

Hearing loss, congenital or acquired (most commonly age-related hearing loss), is a major health issue that affects approximately 30 million people in the United States alone[1] compared to about 5.4 million for Alzheimer's disease.[2] Congenital hearing loss has an incidence of about 1:1,000 births,[3] of which about half have a defined genetic cause. Because the cochlea is surgically accessible and local application into a relatively immune-protected environment is possible, gene therapy using viral vectors is an attractive approach for treating hearing loss. For congenital recessive deafness, gene addition is possible, whereas congenital dominant forms might be treated by silencing or correcting the mutated gene.[4] Gene therapy also holds promise for age-related hearing loss by targeting pathways involved in hair cell (HC) or spiral ganglion neuron survival (e.g., neurotrophic factors[5] or antioxidant proteins[6,7]) or by manipulating gene expression in supporting cells to induce their transdifferentiation into hair cells.[8] For congenital hereditary hearing loss, at least 70 genes are causative in humans. In many cases, they affect the function of hair cells, the receptor cells of the inner ear. The cochlea has two types of hair cells. Inner hair cells (IHCs) convert the mechanical stimulus of sound vibration into a neural signal that is transmitted by type I spiral ganglion neurons to the brain. Outer hair cells (OHCs) connect only to poorly defined type II neurons. Their main function is to amplify the vibration produced by sound by as much as 60 decibels (dB) in a frequency-specific manner, and they are essential for frequency discrimination[9] (important in speech perception). Most deafness genes known to affect hair cell function are expressed in both cell types, so, in general, gene therapy strategy should target both IHCs and OHCs. Hair cells in the vestibular system are essential for our sense of balance and for coordinating eye movements. They are often affected in hereditary deafness so gene therapies should target them as well.

The major limitation of gene therapy for the cochlea is the relative inefficiency of vectors that mediate transgene expression in hair cells. Several gene delivery strategies have targeted sensory cells in the cochlea, including viral and non-viral methods (see Kohrman and Raphael[10] and Sacheli et al.[11] for review). As yet, however, none of these has led to efficient transgene expression in hair cells. Adeno-associated virus (AAV) vectors are presently the most promising vectors for cochlear gene delivery, but in vivo transduction is mostly limited to IHCs. In previous studies,[12,13] virtually no OHCs were transduced by AAV vectors after in vivo injection in mice. Similarly, it is difficult to express genes in hair cells in vitro for research, which has slowed characterization of proteins involved in hair cell function. There is, therefore, a great need for a vector system that effectively

Received 18 November 2016; accepted 5 December 2016;
http://dx.doi.org/10.1016/j.ymthe.2016.12.010.

[6]These authors contributed equally to this work.

Correspondence: David P. Corey, Department of Neurobiology and Hughes Medical Institute, Harvard Medical School, 220 Longwood Avenue, Boston, MA 02115, USA.
E-mail: dcorey@hms.harvard.edu
Correspondence: Casey A. Maguire, Department of Neurology, The Massachusetts General Hospital, Building 149, Charlestown, Boston, MA 02129, USA.
E-mail: cmaguire@mgh.harvard.edu

transduces both IHCs and OHCs, both in vitro and in vivo. It would pave the way to clinical trials, and would also be useful in studying hair cell physiology.

In this work, we tested exosome-associated AAV vectors (exo-AAVs) for delivery to cochlear hair cells and compared different injection routes to the cochlea in mice. Exosomes are cell-derived natural lipid structures involved in intercellular communication and are potential therapeutic carriers of nucleic acids and proteins (see Fitzpatrick et al.[14] and György et al.[15]). We previously observed that exosome association of AAV enhances transduction of cells in vitro and in vivo,[16,17] so we hypothesized that exosomes would also augment gene delivery into cochlear hair cells.

We demonstrate here that exo-AAV vectors are efficient carriers of transgenes into cochlear and vestibular hair cells both in vitro and in vivo. Exo-AAV vectors outperform conventional AAV vectors in gene transfer efficiency and are well tolerated. Furthermore, we show that exo-AAV is useful as a gene therapy system, partially rescuing hearing in a mouse model of human deafness (lipoma HMGIC fusion partner-like 5/tetraspan membrane protein of hair cell stereocilia [*Lhfpl5/Tmhs*$^{-/-}$]).

RESULTS

AAV1 Associates with Exosomes When Vectors Are Isolated from Ultracentrifuged Cell Culture Medium

Of AAV serotypes, AAV1 (the number denotes the capsid serotype) has been reported to be the most effective for cochlear hair cell transduction in preclinical gene therapy studies.[12,13] We therefore prepared exo-AAV1 and conventional AAV1. AAV1 and exo-AAV1 were isolated from the lysate and culture medium of vector-producing 293T cells, respectively (Figure 1A; see Materials and Methods). Using cryoelectron microscopy (cryo-EM) and transmission EM (TEM) in combination with immunogold labeling, we qualitatively observed AAV capsids both bound to the surface of exosomes and in their interiors (Figures 1A and S1A–S1D). The capsids lining the outer exosome membrane could be clearly distinguished as surface bound, whereas capsids that appear "inside" could be above, inside, or below the vesicle within the TEM section. However, we observed instances of capsids distorting the membrane from the interior of the vesicle, directly confirming that at least some of the capsids are indeed on the interior (Figure S1B).

Exo-AAV Outperforms Conventional AAV in Transgene Delivery to Cochlear Hair Cells in Explant Cultures

We first assessed transgene delivery efficiency of conventional AAV1 and exo-AAV1 vectors on cochlear explant cultures. Cochleas were dissected at postnatal day 1 (P1) and placed in organ culture. Vectors were added to the culture medium 1 day later. We used vectors encoding GFP under the strong hybrid cytomegalovirus (CMV)/chicken beta actin (CBA) promoter. After culturing the cochleas with the vectors for 3 days (equivalent to age P5), tissues were fixed, labeled with phalloidin and with antibodies to the hair cell marker myosin VIIa, and viewed with a confocal microscope.

Exo-AAV1 vector was superior to conventional AAV1 vector in gene delivery to hair cells (Figures 1B–1E). At 10^{11} genomic copies (GCs) per cochlea, conventional AAV1-GFP vector transduced approximately 20% of IHCs and OHCs, whereas exo-AAV1-GFP transduced up to 65% of IHCs and 50% of OHCs ($p < 0.001$ and $p < 0.01$, respectively; Figure 1C). We also looked for regional differences in efficiency, and found exo-AAV1 outperformed conventional AAV1 at both the middle and basal turns of the cochlea (Figure 1D; $p < 0.01$ for middle and basal turns, not significant for apical turn).

We also tested another serotype, AAV9, as both exo-AAV9 and conventional AAV9. At 10^{11} GCs/cochlea, we observed a significant enhancement of transduction by exo-AAV9 (Figures 1E and S2A). Strikingly, exo-AAV9 transduced almost 95% of IHCs and OHCs (Figure 1E). We conclude that both exo-AAV1 and exo-AAV9 vectors significantly enhance both IHC and OHC transduction in cochlear explant cultures compared to conventional AAV vectors.

Exo-AAV Outperforms Conventional AAV in Transgene Delivery to Cochlear Hair Cells In Vivo

These results indicate that exo-AAVs can be powerful gene-delivery vehicles for in vitro experimental work, but they may not reflect the in vivo performance needed for therapy. We therefore compared conventional AAV1 and exo-AAV1 in vivo using direct injections into P0/P1 mouse cochleas. We compared two injection routes: through the round window membrane (RWM) into the scala tympani (used in two animal models of hereditary deafness[12,13]), and through the lateral wall of the cochlea by cochleostomy at the basal turn. In both cases, 250 nL of virus-containing solution was injected over ~10 min.

Conventional AAV1-GFP transduced some IHCs but few OHCs. Cochleostomy delivery of conventional AAV1 vector resulted in only 36% GFP-positive IHCs and 17% GFP-positive OHCs (Figures 2A and 2B). Upon RWM injection, we observed more GFP-positive IHCs (up to 65%) but fewer OHCs (~14%) (Figures 2A and 2B). With either route, however, exo-AAV1-GFP vectors significantly enhanced gene delivery. When delivered by cochleostomy, exo-AAV transduced 63% of IHCs and 28% of OHCs. With RWM injection, 88% of IHCs and 25% of OHCs were transduced (Figures 2A and 2B).

As reported by Askew et al.,[13] cochlear injection of P0 mouse pups is difficult, causing significant variability in transduction. Our results (Figures 2B–2D) include all of the injected mice ($n = 38$ for cochleostomy; $n = 23$ for RWM), even those with very low transduction efficiency that may result from unsuccessful injection. In our best injections with exo-AAV vectors, we observed >95% IHCs and ~50% OHCs transduced with our working dose (250 nL, containing 5×10^9 genomic copies of AAV). The best cases of the cochleostomy and RWM injections had similar hair cell transduction rates.

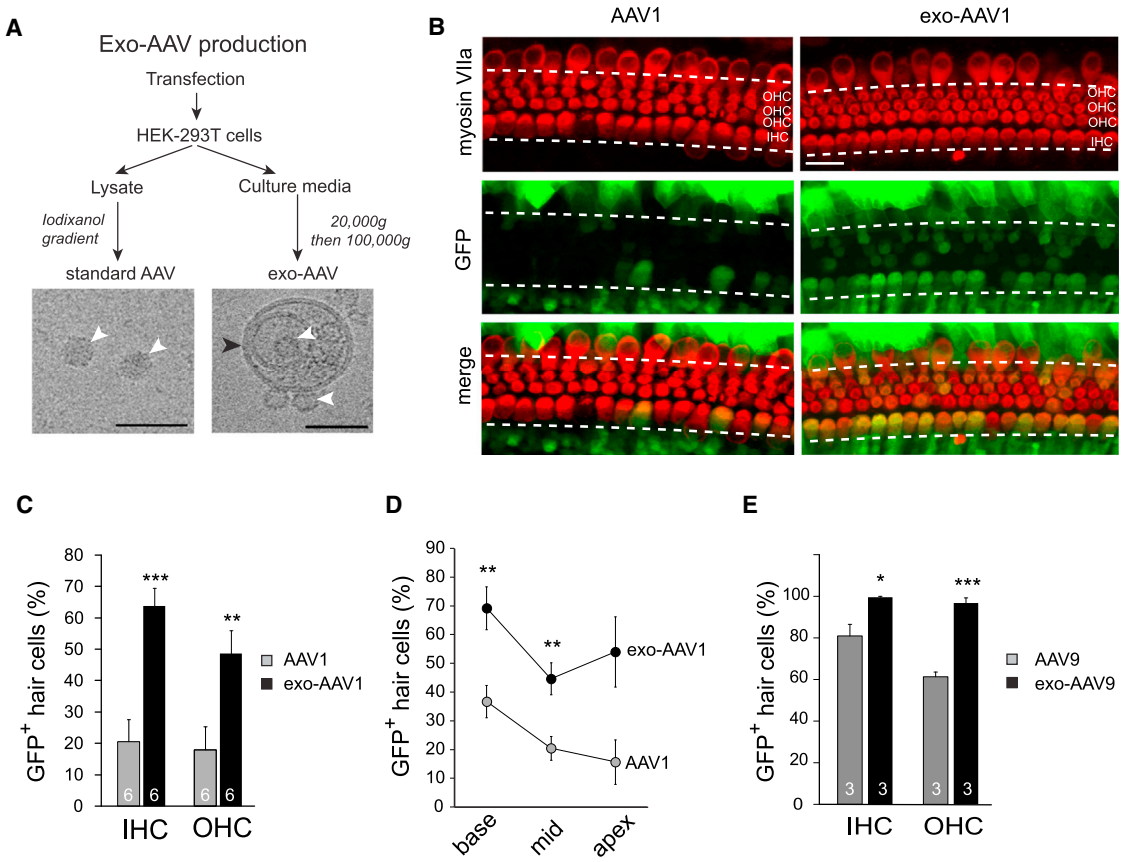

Figure 1. Exo-AAV Outperforms Conventional AAV in Hair Cell Transduction in Culture

(A) Standard (conventional) AAV and exo-AAV production workflow. AAV was purified from HEK293T cell lysate, whereas exo-AAV was isolated from the culture medium of the cells. Cryoelectron microscopy shows AAV1 capsids associated with exosomes. White arrowheads show AAV capsids, whereas the black arrowhead indicates the lipid membrane. Scale bars, 50 nm. (B) Transduction of cochlear whole mount cultures with AAV1-CBA-GFP or exo-AAV1-CBA-GFP. Cochleas were explanted from CD1 mice at P1. Vectors were added (10^{11} GCs) the following day and incubated overnight. Organs were cultured for 3 more days. Exo-AAV1-GFP shows efficient transduction of IHCs and OHCs. Hair cells were labeled with anti-myosin VIIa antibody. Scale bar, 20 μm. (C) Proportion of GFP-positive hair cells in cochleas transduced with 1×10^{11} GCs of conventional AAV1 or exo-AAV1. Numbers in the bars represent the number of cochleas. Three images were taken for each cochlea (base, middle, and apex; fields chosen by distance). Mean ± SEM; ***$p < 0.001$, **$p < 0.01$, one-tailed t test. (D) Proportion of GFP-positive hair cells in different regions of the cochlea (basal, middle, and apical turns) transduced with conventional AAV1 or exo-AAV1. n = 6 cochleas for each data point; **$p < 0.01$, one-tailed t test. Mean ± SEM. (E) GFP-positive hair cells in cochleas transduced with 1×10^{11} GCs of conventional AAV9 or exo-AAV9. Mean ± SEM; ***$p < 0.001$, *$p < 0.05$, one-tailed t test.

However, in our hands, cochleostomy results were more variable and there were more instances with very low GFP expression.

Because GFP expression in individual hair cells may vary with multiple AAV genomes being delivered, we quantified GFP intensity using automated image analysis. Among GFP-positive IHCs, average GFP fluorescence intensity per cell was 70% higher with exo-AAV than with conventional AAV, with either cochleostomy or RWM injection ($p < 0.01$ for cochleostomy and $p < 0.05$ for RWM injection; Figure 2C). For OHCs, no significant difference in GFP intensity per cell was evident between exo-AAV1 and conventional AAV1.

For cochleostomy, transduction rates varied with distance from the injection site. We counted more transduced hair cells in the base (near the injection site) than in the apex (Figure 2D). The gradient was particularly steep and significant for OHCs, with only a few OHCs transduced at the apex (repeated-measures ANOVA for the entire dataset to analyze the relationship between location and transduction; $p = 0.0009$ for AAV1 and $p = 0.02$ for exo-AAV1). With RWM injection, however, there was no significant gradient, suggesting that the virus can diffuse more freely with this approach. Overall, in all subregions tested, with both injection routes, exo-AAV1 significantly outperformed conventional AAV1 (Figure 2D).

With cochleostomy injections of either conventional or exo-AAV1, we also observed robust expression of GFP in spiral ganglion neurons, cells in the inner sulcus, Claudius cells, and Hensen cells (Figure S3).

Surprisingly, GFP-positive hair cells were also evident in the utricle and in the ampullas of the lateral semicircular canals following

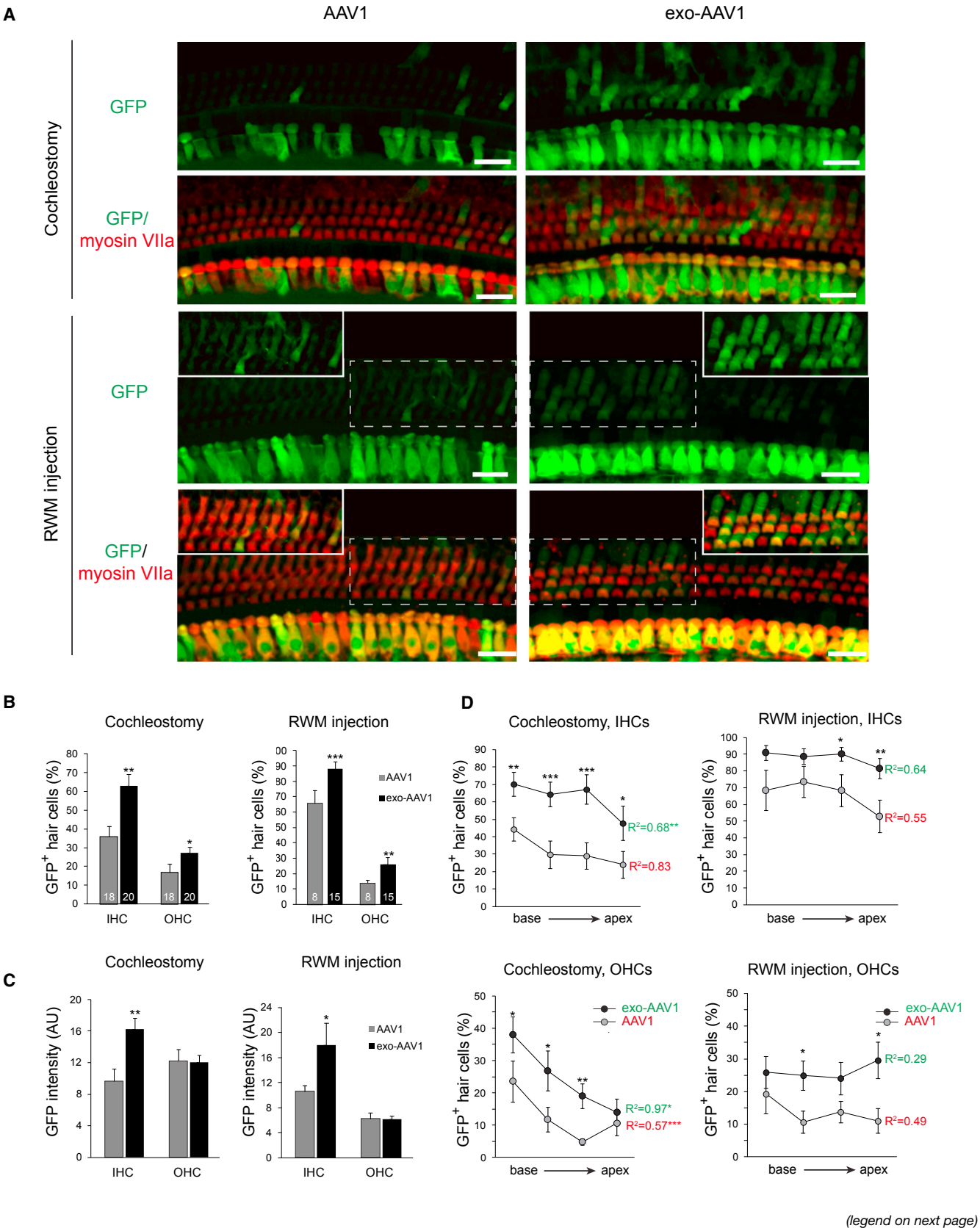

(legend on next page)

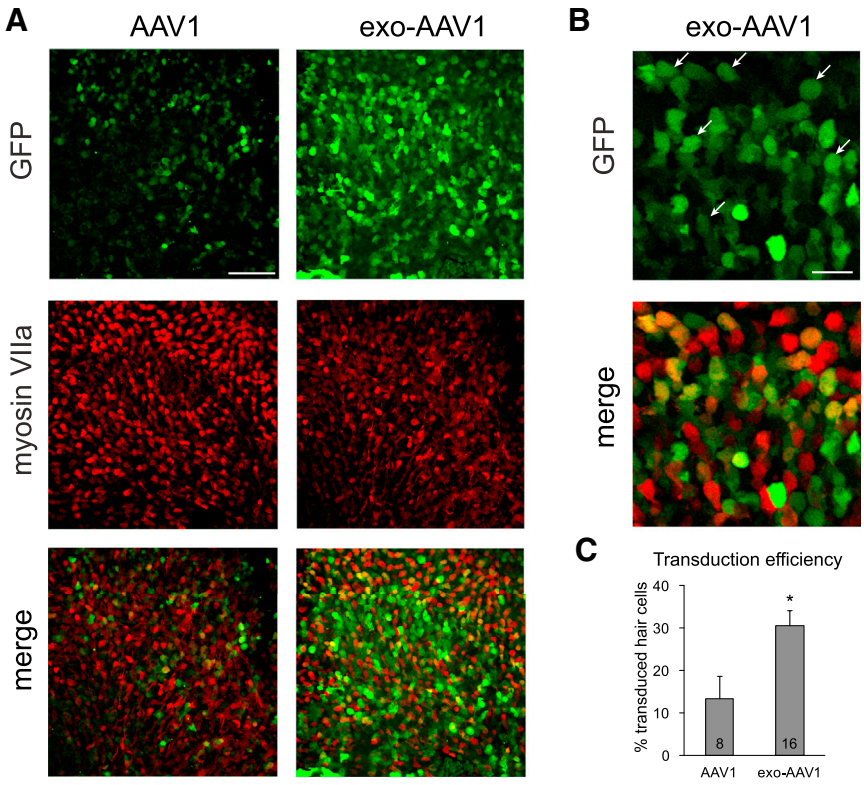

Figure 3. Exo-AAV1 Transduces Utricular Hair Cells after RWM Injection

CD1 mice were injected with 5×10^9 GCs of conventional AAV1-CBA-GFP or exo-AAV1-CBA-GFP. (A) GFP indicates all transduced cells; myosin VIIa labels just hair cells. Scale bar, 40 μm. (B) Higher magnification shows many transduced cells identified also express myosin VIIa (white arrows). Scale bar, 20 μm. (C) Blinded unbiased quantification of transduced hair cells. Mean ± SEM. $p < 0.05$, Mann Whitney U test. Numbers in the boxes indicate the number of biological replicates.

exo-AAV administration by either cochleostomy (Figure S4) or RWM injection (Figures 3A and 3B). In the utricle after RWM injection, exo-AAV1 transduced 30% of hair cells (Figure 3C), 2.3 times more than conventional AAV1 ($p < 0.05$, Mann Whitney U test), indicating some level of diffusion throughout endolymphatic compartments at that age. Several myosinVIIa-negative cells (supporting cells) were also transduced with either vector. Thus, exo-AAV vectors also have the potential for gene delivery to the vestibular system.

Because exo-AAV9 outperformed exo-AAV1 in vitro, we also tested AAV9 in vivo. Transduction rates in vivo were similar between exo-AAV1 and exo-AAV9, with AAV9 targeting 60% of IHCs and 25% of OHCs after injection (Figure S2B).

Exo-AAV1 Gene Delivery Partially Rescues Hearing in *Lhfpl5*$^{-/-}$ Mice

We next tested the ability of exo-AAV to produce efficient expression of a biologically relevant gene, asking whether exo-AAV1 could improve hearing in a mouse model for human hereditary deafness. We selected a mouse with a targeted deletion of *Lhfpl5* (also known as *Tmhs*). LHFPL5 protein is an integral component of the mechanotransduction machinery in both OHCs and IHCs, and its absence leads to early hair cell degeneration, profound deafness, and severe vestibular dysfunction.[18] Because this model is on the C57BL/6 background and our previous gene transfer experiments were performed on CD1 mice, we tested whether exo-AAV transduces hair cells with the same efficiency on the C57BL/6 background. We did not observe any differences between CD1 and C57BL/6 transduction rates using exo-AAV1-GFP (Figure S5). Although results were variable, we noted that some of the C57BL/6 animals showed very efficient transduction (>95% IHC and >85% OHC transduction; Figure S6), which was never achieved with conventional AAV1.

For gene-addition therapy, a mouse-codon-optimized gene encoding LHFPL5 with a hemagglutinin (HA) tag at the N terminus was cloned into an AAV vector backbone under the CBA promoter (Figure S7A). When this exo-AAV1-HA-*Lhfpl5* was produced in HEK293T cells,

Figure 2. Exo-AAV Outperforms Conventional AAV in Hair Cell Transduction In Vivo

CD1 mice were injected at postnatal day 1 with 5×10^9 GCs of conventional AAV1-CBA-GFP or exo-AAV1-CBA-GFP either by cochleostomy or through the round window membrane. (A) Efficient OHC transduction by exo-AAV1 compared to conventional AAV1. The insets in the lower panels show the outlined region of the main panel at the same magnification, but with higher brightness. All image post-processing was done identically between AAV1 and exo-AAV1. Scale bars, 20 μm. (B) Proportion of GFP-positive hair cells in cochleas transduced with conventional AAV1 versus exo-AAV1. Numbers in the boxes represent the number of injected animals. Eight images were acquired for each sample, and four were analyzed. Mean ± SEM; ***$p < 0.001$, **$p < 0.01$, *$p < 0.05$, one-tailed t test. The experiment was carried out on separate occasions using three different litters for each vector and different exo-AAV preparations, with 38 mice/cochleas in total. For RWM injection, we performed the injections on two separate litters for each vector (23 mice/cochleas in total). Bars represent the combined results from all animals. (C) GFP fluorescence intensity in GFP-positive hair cells. Hair cells were identified by myosin VIIa fluorescence-based segmentation (Imaris); n = 6 cochleas for cochleostomy in each group, and n = 4 for RWM injection in each group. Four images were analyzed per cochlea. GFP-negative (GFP level below +2 SD background) cells were excluded from the intensity analysis. Mean ± SEM. (D) Percentage of GFP-positive hair cells in four regions of the cochlea (base, midbase, midapex, and apex), transduced with conventional AAV1 or exo-AAV1. Mean ± SEM); ***$p < 0.001$, **$p < 0.01$, *$p < 0.05$, Mann Whitney U test between AAV1 and exo-AAV1. R^2 is the coefficient of determination for the average values in each region. It tests whether there is a correlation between the location and transduction efficiency. Most conditions showed more transduction in the base for cochleostomy but not for RWM injection. Repeated-measures ANOVA test assuming equal sphericity; ***$p < 0.001$, **$p < 0.01$, *$p < 0.05$.

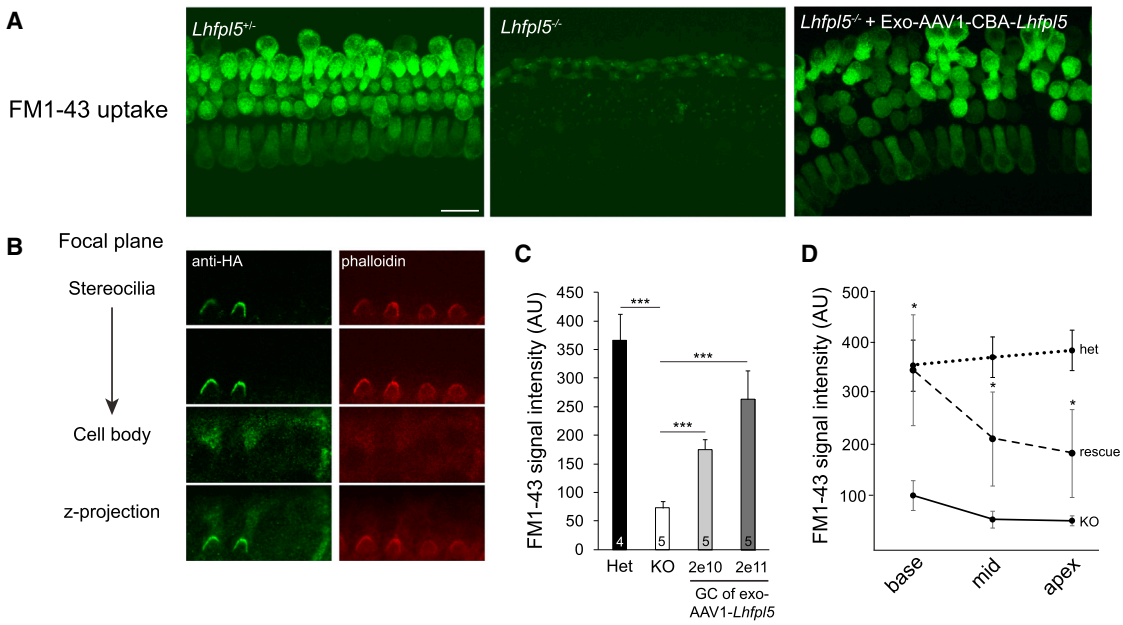

Figure 4. Exo-AAV1-*HA-Lhfpl5* Rescues FM1-43 Loading in Hair Cells in Culture

Lhfpl5$^{+/-}$ *or Lhfpl5*$^{-/-}$ cochleas (C57BL/6 background) were dissected at P0 and placed into culture for 8 days. Exo-AAV1-HA-*Lhfpl5* was added to the culture at P0. At P8, (*Tmc2*) is no longer expressed and so is no longer an alternate path for FM1-43 loading. (A) FM1-43 loading indicating functional hair cells in control *Lhfpl5*$^{+/-}$ mice. Knockout transmembrane channel like 2 *Lhfpl5*$^{-/-}$ animals showed no loading, but loading was evident in the *Lhfpl5*$^{-/-}$ animals after vector administration (2×10^{11} GCs). Scale bar, 20 μm. (B) LHFPL5 in stereociliary bundles of KO mice after vector-mediated *Lhfpl5* gene delivery, which was revealed with anti-HA staining. Hair bundle actin was labeled with phalloidin (red). (C) FM1-43 signal intensity measured with ImageJ. Het, *Lhfpl5*$^{+/-}$ KO, *Lhfpl5*$^{-/-}$ GC, genomic copes. Exo-AAV1-CBA-HA-*Lhfpl5* administration led to increased FM1-43 signal intensity. ***$p < 0.001$, t test. Mean ± SEM. (D) FM1-43 signal intensity in *Lhfpl5*$^{+/-}$, *Lhfpl5*$^{-/-}$, and exo-AAV1-HA-*Lhfpl5*-rescued *Lhfpl5*$^{-/-}$ animals (2×10^{11} GCs) in different regions of the cochlea. *$p < 0.05$, t test. Mean ± SEM.

anti-HA immunoblotting of cell lysates revealed bands of the expected molecular weight for LHFPL5 (Figure S7B).

Next, we tested whether this construct restores function in cochlear explant cultures from *Lhfpl5*$^{-/-}$ animals. Exo-AAV1-HA-*Lhfpl5* restored FM1-43 loading in explant cultures (indicating the presence of functional mechanotransduction channels) (Figure 4A). In addition, anti-HA labeling was present in hair cell stereocilia (Figure 4B). We quantified average FM1-43 signal in cochlear explants from *Lhfpl5*$^{+/-}$ mice, *Lhfpl5*$^{-/-}$ mice, and *Lhfpl5*$^{-/-}$ mice transduced in culture with two different doses of exo-AAV1-HA-*Lhfpl5*. The average FM1-43 fluorescence intensity per hair cell in *Lhfpl5*$^{-/-}$ cochlea was comparable to the background intensity in an area without hair cells. In *Lhfpl5*$^{-/-}$ cochleas transduced by exo-AAV1-HA-*Lhfpl5* vector, FM1-43 intensity was 70% of the *Lhfpl5*$^{+/-}$ positive control at the highest tested dose (Figure 4C). FM1-43 intensity increased from apex to base in exo-AAV1-HA-*Lhfpl5*-treated *Lhfpl5*$^{-/-}$ cultures, a gradient similar to that seen with the GFP reporter (Figure 1D). At all points, cellular FM1-43 intensity levels were significantly higher than in untreated *Lhfpl5*$^{-/-}$ cultures (Figure 4D). At the base, FM1-43 intensity was as high in exo-AAV1-HA-*Lhfpl5*-treated *Lhfpl5*$^{-/-}$ cultures as in heterozygous positive controls (Figure 4D). These data confirmed that the construct was functional and that the HA tag allowed specific detection of the transgene.

Next, we injected exo-AAV1-*HA-Lhfpl5* into the cochlea by RWM injection at P1 to P2. RWM injection was used rather than cochleostomy because it was less variable in our hands. Furthermore, we could use a higher volume and therefore dose using RWM injection, and there was less of base-to-apex decrease in transduction with RMW injection compared to cochleostomy (Figure 2D). For in vivo injection, we administered the maximum injectable volume based on preliminary experiments: 1,200 nL (containing 2.7×10^9 GCs). Several days later, we dissected cochleas and cultured them for 1 to 2 days before viewing. Anti-HA immunostaining at P4+2 showed distinct signal in stereociliary bundles of both IHCs and OHCs (Figure 5A). High magnification images revealed anti-HA staining at the tips of stereocilia, including the tallest row, in agreement with the previously reported localization of native LHFPL5[18] (Figure 5B). We confirmed that exo-AAV-transduced IHCs and OHCs have functional mechanotransduction, as assessed by FM1-43 loading (Figure 5C). We assessed the efficiency of exo-AAV transduction by counting the hair cells with anti-HA labeling at the bundle and found that 72 ± 17% of IHCs and 30 ± 5% of OHCs exhibited bundle staining, with nearly equal distribution along the cochlea (Figure 5D).

We also tested AAV-*HA-Lhfpl5*-internal ribosomal entry site (IRES)-*GFP* packaged in exo-AAV1. This allows co-expression of LHFPL5

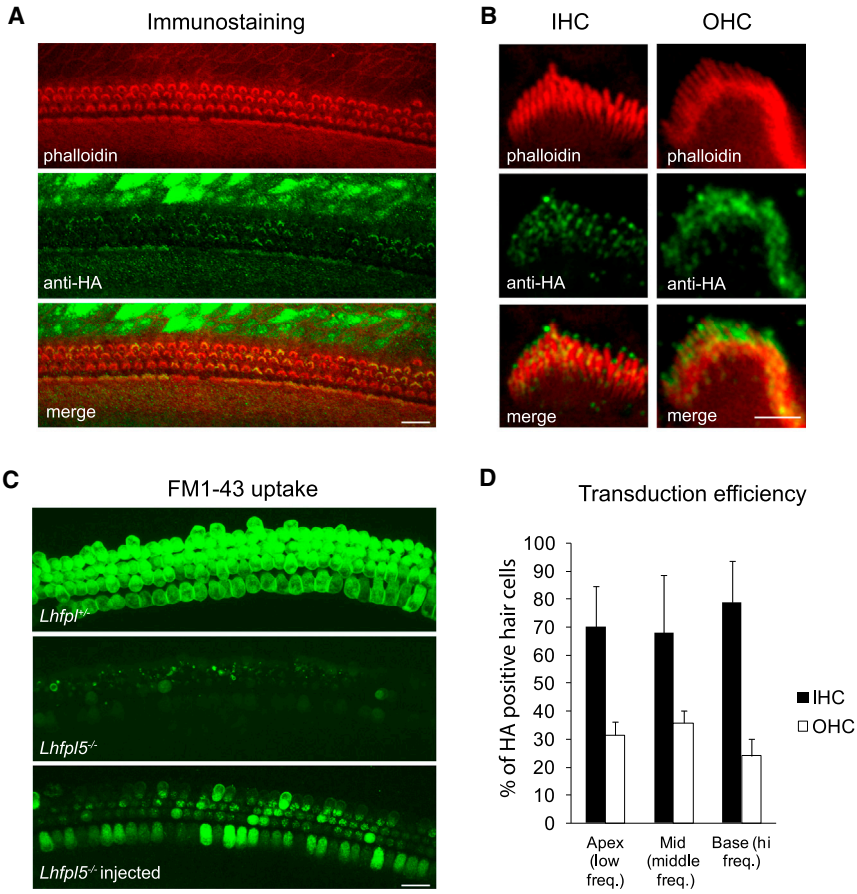

Figure 5. RWM Injection of Exo-AAV1-*HA-Lhfpl5* Induces LHFPL5 Bundle Expression in Hair Cells and Rescues FM1-43 Loading

(A) HA-LHFPL5 detected with immunolabeling for the HA tag. Cochleas from *Lhfpl5*$^{-/-}$ *mice* (C57BL/6 background) were injected through the round window at P1 with exo-AAV1-CBA-HA-*Lhfpl5*. Hair bundle actin was stained with phalloidin (red). HA staining is apparent in the IHC and OHC bundles as well as in some supporting cells. P4+2 days in culture. Scale bar, 20 μm. (B) High magnification images show anti-HA staining in the bundles of an inner hair cell and an outer hair cell. Anti-HA staining is detectable at the tips of all rows of stereocilia. Scale bar, 2 μm. (C) RWM injection of exo-AAV1-CBA-HA-*Lhfpl5* through the round window at P1 restores FM1-43 loading in IHCs and OHCs (7 days after injection; P6+2). Scale bar, 20 μm. (D) Regional transduction efficiency based on HA staining in bundles of the apical, middle, and basal regions of the cochlea (P4+2) (n = 4). No difference was apparent between different regions.

and GFP in the same cell. Importantly, all GFP-positive cells exhibited anti-HA staining, confirming specificity of the anti-HA antibody (Figure S8). Some GFP-negative cells also showed anti-HA bundle staining, which may be due to weak translation downstream of the IRES, making GFP undetectable.

To determine whether exo-AAV-mediated gene transfer impairs normal hearing, we tested heterozygous animals injected with exo-AAV1-*HA-Lhfpl5* by RWM injection. RWM injection did not alter hearing thresholds, as measured by auditory brainstem evoked responses (ABRs) (Figure 6B) or change ABR P1 or P2 peak amplitudes (Figure 6C), confirming that both the procedure and the vectors are safe at early ages.

Next, we tested physiological rescue of hearing in deaf mice injected with exo-AAV1-*HA-Lhfpl5* and performed ABR recordings at 4 weeks post-injection using frequencies from 4 to 45 kHz (Figures 6A–6C). Uninjected *Lhfpl5*$^{-/-}$ animals did not show detectable ABRs at any sound pressure level (SPL) up to 100 dB (Figure 6A). In *Lhfpl5*$^{-/-}$ animals injected through the RWM with exo-AAV1-*HA-Lhfpl5*, we observed improved hearing thresholds at frequencies from 4 to 22 kHz (Figure 6B) in 9 out of 12 animals. The four animals with the best rescue showed thresholds of ~70 dB SPL at 8 and 11 kHz, an improvement of ~30 dB. We never detected ABRs for sound presented to the non-injected side. Although we did not directly analyze gene transfer in the non-injected ear, the ABR data suggest that any gene transfer to the contralateral ear is minimal using this injection protocol. Nevertheless, we have previously reported low levels of gene transfer to inner ear hair cells after intravenous injection of exo-AAV in adult mice, suggesting that it may be possible to transduce both ears under certain conditions.[19]

The average peak 2 amplitudes at 90 dB SPL were 0.88 ± 0.18 and 0.84 ± 0.12 μV (mean ± SEM) at 8 and 11 kHz, respectively, which is approximately 25% of those in normal heterozygotes (Figure 6C). Latencies of peak 1 and peak 2 were not significantly increased in rescued animals compared to wild-type (WT) animals at the same SPL, except at 11 kHz for peak 1 (Figure 6C; $p < 0.01$, two-tailed t test). Injected and non-injected heterozygotes did not show a statistically significant difference in the latency of the P1 or P2 ABR peaks (Figure 6C).

We tested the behavioral correlates of hearing and balance in Lhfpl5 knockouts (KOs) rescued with exo-AAV. We first found that rescue of hearing by exo-AAV1-*HA-Lhfpl5* was sufficient to elicit a startle response to a loud clap, a standard test of hearing (Movie S1).

Head bobbing and circling are common traits of *Lhfpl5* KO mice and may reflect abnormal vestibular function.[20–22] Because GFP-positive hair cells were also evident in vestibular sensory epithelia, suggesting vector diffusion to the vestibular system (Figure 3), we performed behavioral tests in treated (injected through the RWM with exo-AAV1-HA-*Lhfpl5)* and nontreated *Lhfpl5* KO mice. We performed

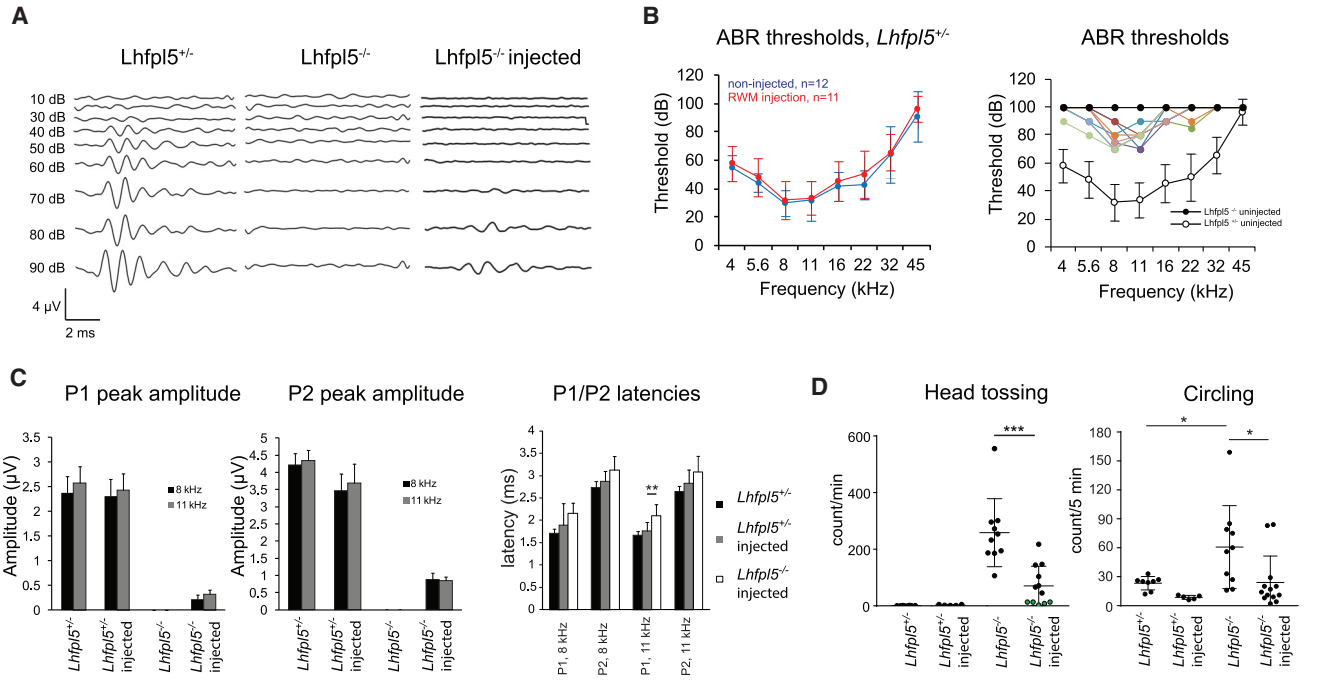

Figure 6. RWM Injection of Exo-AAV1-HA-*Lhfpl5* Improves Hearing and Improves Movement Abnormalities in *Lhfpl5*$^{-/-}$ Animals

(A) ABR waveforms at 8 kHz from heterozygous, uninjected *Lhfpl5*$^{-/-}$ and exo-AAV1-CBA-HA-*Lhfpl5*-injected *Lhfpl5*$^{-/-}$ animals. Sound pressure level is shown in dB. ABR was recorded at 4 weeks post-injection. (B) ABR thresholds (mean ± SD). Left: heterozygous control mice injected with exo-AAV1-CBA-HA-*Lhfpl5* through round window membrane injection. Thresholds were not changed by exo-AAV injection. Right: *Lhfpl5*$^{-/-}$ knockout mice injected with exo-AAV1-CBA-HA-*Lhfpl5* through the RWM at P1. Solid black circles represent uninjected *Lhfpl5*$^{-/-}$ ears and show no detectable ABR at any sound pressure level. Open circles show heterozygous control thresholds at this age (data from left panel non-injected). Colored symbols represent nine individual animals that showed some level of rescue after exo-AAV1-CBA-HA-*Lhfpl5* injection. (C) Peak 1 (P1) and peak 2 (P2) ABR wave amplitudes and latencies at 8 and 11 kHz. ABR peaks were normal in both uninjected and injected control heterozygotes, but were never detected in uninjected knockout animals. ABR peaks were smaller but present in exo-AAV1-injected knockouts. Waveforms were measured at 4 weeks post injection. $p < 0.01$, t test. Mean ± SD. (D) Behavior tests to monitor movement abnormalities in treated and untreated mice. Left: head tossing was quantified by blinded investigators. Head tossing in exo-AAV1-CBA-HA-*Lhfpl5*-injected knockouts was less than in uninjected knockouts, and not detected at all in 5 out of 12 injected animals (green circles). Right: circling was also decreased in exo-AAV1-CBA-*HA-Lhfpl5*-injected knockouts. Circling was quantified using EthoVision XT software, and full 360° turns were identified as a circle. *$p < 0.05$, ***$p < 0.001$, Mann Whitney U test. Mean ± SD.

an open field test, in which animals were placed in a circular arena for 5 min. Normal heterozygous mice showed gait and head stability and normal explorative behavior (Movie S2). On the contrary, *Lhfpl5*$^{-/-}$ mice exhibited frequent head tossing, gait instability, backward movement, and circling. Five out of 12 exo-AAV1-HA-*Lhfpl5*-treated *Lhfpl5*$^{-/-}$ animals did not exhibit head tossing, indicating rescue of balance function. Averaging all animals, we found head tossing was significantly decreased in the treated *Lhfpl5*$^{-/-}$ animals compared to the untreated animals (Figure 6D) ($p < 0.001$, Mann-Whitney U test). Similarly, circling was analyzed using computerized image analysis. Treated *Lhfpl5*$^{-/-}$ animals exhibited significantly fewer 360° rotations compared to untreated animals (Figure 6D) ($p < 0.05$, Mann-Whitney U test). These results confirm that hearing and the abnormal movements characteristic of compromised balance in these mice are improved after exo-AAV1-HA-*Lhfpl5* gene therapy.

DISCUSSION

In this study, we found that exosome-associated AAV transduces cochlear and vestibular hair cells with much greater efficiency than do conventional AAV vectors. Prior studies had shown some transduction of IHCs with conventional AAVs, but little transduction of OHCs.[12,23] We found that exo-AAV1 efficiently transduces IHCs and transduces OHCs much more efficiently than does conventional AAV1. AAV1 was our standard of comparison because it has been used in prior studies of hearing gene therapy.[12,13] In those studies, it was shown to only transduce inner hair cells relatively efficiently. Interestingly, we found that exo-AAV9-GFP was extremely efficient at transduction of cochlear explant cultures, although, in vivo, this serotype performed similarly to exo-AAV1.

In order to determine whether the efficient reporter gene levels in HCs achieved with exo-AAV could be translated to expression of HC-relevant genes, we tested exo-AAV-mediated expression of *Lhfpl5* in deaf *Lhfpl5*$^{-/-}$ mice. After RWM injection, we found widespread expression of HA-tagged LHFPL5 throughout the cochlea. Treated *Lhfpl5*$^{-/-}$ mice were able to respond to sound, as measured physiologically, and showed improvements in balance-related abnormal movement, assessed behaviorally.

Although this is an important step forward in strategies of gene therapy for deafness, hearing restoration was not complete. It may be that the window of therapeutic intervention is limited for *Lhfpl5*. LHFPL5 is expressed in mice beginning about E16.5, and hair cell degeneration in the knockout is evident by P8,[24] so we may not have expressed the transgene soon enough (mice were injected with vector at P0 or P1). It may also be that the HA tag, used for immunostaining, interfered to some extent with the protein function. An untagged *Lhfpl5* could be expressed in future studies. Nevertheless, we achieved hearing thresholds that were 20 dB better than in a recent rescue of *Tmc1* deficiency with conventional AAV1.[13] Although we did not test distortion product otoacoustic emissions (DPOAEs), a measure of OHC function in vivo, we did confirm OHC transduction by immunostaining for the HA tag and FM1-43 loading. Further DPOAE measurements will be necessary to confirm functional OHC mechanotransduction. Interestingly, the best rescue was in the 8–11 kHz range, as also found by Askew et al.[13] Vector transduction efficiency was relatively even along the cochlea, so this frequency-dependent rescue could be because mouse hearing is normally most sensitive in that range.

In a similar study, Akil et al. used a conventional AAV vector to achieve robust hearing rescue in VGLUT3 KO mice.[12] However, the VGLUT3 KO only affects inner hair cells, not outer hair cells, and so is easily rescued by conventional AAV1. Indeed, the authors show that virtually no outer hair cells were transduced with conventional AAV1. In contrast, exo-AAV allows efficient transduction of outer hair cells as well, and is thus applicable to the great majority of deafness genes that are required for function in both inner and outer hair cells. In gene therapies in which both hair cell types require correction, conventional AAV1 will likely not suffice.

The published behavioral phenotype of *Tmhs* (*Lhfpl5*) mutant mice is circling and abnormal head movements, such as shaking and tossing, which are indicative of a balance disorder.[24] We observed that exo-AAV1-*HA-Lhfpl5*-treated *Lhfpl5* KO mice had improvements in both circling and head tossing behavior. We also observed robust transduction of hair cells in the vestibular system in these mice. Together, this may suggest a rescue of balance dysfunction in these mice, although further testing using measurements such as vestibular evoked potentials (VsEPs) could be done to confirm this.

We used self-complementary (sc) AAV vector genomes in our transduction comparisons between exo-AAV and AAV (Figures 2 and 3) as well as for rescue experiments (Figure 6). Sc genomes are genetically engineered variants of the natural single-stranded (ss) AAV genome,[25,26] which give rise to complementary, half-sized AAV genomes that fold into a double-stranded-like structure. Sc genomes are thought to bypass the second-strand synthesis step required for transcription of transgenes from ssAAV vectors. Bypassing this step generally leads to an earlier onset and more robust level of transgene expression, although it comes with the cost of reduced cassette size (~2.4 kb compared to 4.7 kb for ss vectors). That said, many genes fit into sc vectors, including *Lhfpl5*, and a scAAV vector is in clinical trials for the treatment of spinal muscular atrophy (clinicaltrials.gov). It may be promising for certain deafness genes.

Exo-AAV is relatively easy to purify,[19] allowing rapid production of several different constructs for experimental testing. In contrast, purification of conventional AAV is a more complicated and time-consuming process. Also, it is important to note that if new AAV capsids with enhanced transduction in hair cells are discovered, they can be incorporated into the exo-AAV system for a potentially even better performance.

In conclusion, we show that exo-AAV vectors are efficient delivery vehicles for mammalian hair cells of the inner ear, both in vitro and in vivo. Exo-AAV-mediated genetic modification of inner and outer hair cells should facilitate elucidation of the basic biology of hair cells, and represents a promising avenue for gene therapy for human hereditary deafness.

MATERIALS AND METHODS

Animals

All experiments were performed in compliance with ethical regulations and approved by the Animal Care Committee of Harvard Medical School. For in vitro and in vivo studies, we used CD1 mice (Charles River), which were housed and bred in the animal facility at Harvard Medical School. Wild-type C57BL/6 animals were ordered from Charles River. *Lhfpl5* heterozygous and homozygous KO animals were housed and bred in our facility. Male and female mice were randomly chosen for study. Pilot experiments allowed us to estimate the sample size for the animal experiments.

Genotyping

For genotyping, we used the following primers: wild-type exon 2 forward: TGACTGCTGGATCTCAGTGC; wild-type exon 2 reverse: GTTTGGCTGCTGGTCTTAGC; Lhfpl5 KO forward: TAGCAGGCATGCTGGGGATG; *Lhfpl5* KO reverse: TCCGCTGATGGCC TTTCTCA. PCR conditions were as follows: 95°C for 2 min, followed by nine cycles of 95°C for 30 s, 66°C for 30 s (−1°C/cycle), and 72°C for 30 s, then 25 cycles of 95°C for 30 s, 57°C for 30 s, and 72°C for 30 s, and finally 75°C for 5 min. The PCR products were separated on an agarose gel. *Lhfpl5*$^{-/-}$ allele shows a 238-bp band. Wild-type allele shows a 577-bp band.

Vector Preparation

We isolated conventional AAV and exo-AAV vectors from transfected HEK293T cells, as previously described.[16,17] For each production, we plated two 15-cm tissue culture dishes with 1.5×10^7 HEK293T cells. The next day, cells were transfected using the calcium phosphate method, with the adenovirus helper plasmid (pAdΔF6,[27] 26 μg), rep/cap plasmid (pXR1[28] for AAV1, pAR9 for AAV9, 12 μg) and inverted terminal repeats (ITR)-flanked transgene cassette plasmid (10 μg) to induce production of AAV. All plasmids were obtained from the Massachusetts General Hospital virus vector core. Plasmids were diluted in 780 μL with 2.5 mM HEPES and 2 M calcium chloride and then added drop-wise into 780 μL 2x

HEPES-buffered saline (280 mM NaCl, 50 mM HEPES, and 1.5 mM Na_2HPO_4, pH 7.04) while vortexing in 15-mL tubes. The mixture was incubated at room temperature for 20 min before adding it to cells drop-wise. The day after transfection, medium was changed to DMEM containing 2% fetal bovine serum (FBS). The following day, medium was changed to DMEM containing 2% exosome-free FBS (made by overnight 100,000 × *g* ultracentrifugation to deplete bovine exosomes). Exo-AAV vectors were isolated from the media 3 days after transfection using differential centrifugation as described before.[16] Cells were depleted at 300 × *g* for 5 min and 1,000 × *g* for 10 min. Next, larger extracellular vesicles (apoptotic bodies, microvesicles) were removed by a 20,000 × *g* spin for 60 min. The supernatant from the 20,000 × *g* spin was subjected to 100,000 × *g* centrifugation using a type 70 Ti rotor in an Optima L-90K ultracentrifuge for 1.5 hr (both Beckman Coulter). The exosome pellet was re-suspended in serum-free, antibiotic-free DMEM medium. Conventional AAVs were purified from the cell lysate using iodixanol-gradient ultracentrifugation. Vectors were stored at −80°C until use. For titration of exo-AAV vectors, we first treated the titration aliquot with DNase to remove plasmid DNA. Next, we isolated all capsid-protected nucleic acids from the sample using the Roche High Pure Nucleic Acid viral kit (Roche) in order to remove PCR inhibitors and nucleases potentially present in exosome preparations and to fully lyse the exosomal membrane. For titration of conventional AAV, we have observed that the DNase I treatment and downstream nucleic acid purification steps are not required because the crude cell lysates are treated with Benzonase nuclease to remove plasmid DNA. Titration of standard AAV by simply diluting the sample before titration or using the DNase I/Roche High Pure Nucleic Acid viral kit procedure, as for exo-AAV, yielded identical titers. Finally, we quantified AAV genomic copies in conventional and exo-AAV preparations using TaqMan qPCR with BGH polyA-sequence specific primers and probe.[17] Titers for all vectors (AAV and exo-AAV) were in the $2 \times 10^{12} - 1.5 \times 10^{13}$ GCs/mL range.

AAV Vector Constructs

AAV transgene plasmid (AAV2 inverted terminal repeat [ITR] flanked) encoding GFP under the hybrid CMV immediate-early/CBA promoter, AAV-CBA-GFP, was kindly provided by Dr. Miguel Sena-Esteves (UMass Medical Center). AAV-CBA-GFP is a sc genome. pAdΔF6,[27] pXR1[28] (AAV1), and AAV9 plasmids were all obtained from the Massachusetts General Hospital virus vector core. We constructed two AAV vectors encoding murine *Lhfpl5*. The transgene was designed from the coding region of mRNA of *Mus musculus Lhfpl5* (NCBI reference sequence: NM_026571.2). A mouse-codon-optimized version of mouse *Lhfpl5* with an N-terminal human influenza HA tag was synthesized and inserted into a cloning vector (pUC57-Kan) by Genscript. To construct this plasmid, we first digested sc-AAV-CBA-GFP with HindIII and NheI to remove the GFP transgene. The pUC57-Kan plasmid was similarly digested to release codon-optimized, HA-tagged *Lhfpl5*. This insert was ligated with the scAAV backbone to create scAAV-CBA-HA-*Lhfpl5*. A second construct was made using an ss AAV plasmid as the backbone. For this construct, we used the plasmid ssAAV-CBA-IRES-GFP, which was kindly provided by Dr. Miguel Sena-Esteves. This plasmid contains a multiple cloning site after the CBA promoter and an IRES-driven GFP, allowing for co-expression of GFP and a gene of interest. We digested ssAAV-CBA-IRES-GFP with SpeI and NheI, and dephosphorylated the plasmid with calf inositol phosphatase before agarose gel purification. We PCR amplified HA-*Lhfpl5* from scAAV-CBA-HA-*Lhfpl5* using forward and reverse primers flanked with SpeI and NheI recognition sequences, respectively. The amplified product was digested overnight with SpeI and NheI and ligated with similarly digested ssAAV-CBA-IRES-GFP. After restriction digest screening for correct ligation orientation, ssAAV-CBA-HA-*Lhfpl5*-IRES-GFP was generated. Confirmational DNA sequencing was performed.

Transmission Electron Microscopy

Exo-AAV vectors were pelleted and fixed for 30 min in 4% formaldehyde in PBS. The pellet was cryoprotected in 2.3 M sucrose in PBS before it was frozen in liquid nitrogen. Cryosections (approximately 80 nm thick) were incubated with 1:100 dilutions of mouse anti-AAV1 antibody, which recognizes intact capsids (Clone ADK1a; American Research Products), followed by a 10-nm gold-conjugated secondary anti-mouse antibody (Sigma-Aldrich). Images were acquired with a Tecnai G^2 Spirit BioTWIN transmission electron microscope (FEI Company) in the Harvard Medical School Electron Microscopy Facility.

Cryo-EM

Cryo-EM was performed on conventional and exo-AAV1 vectors. Briefly, 4 μL of sample was deposited on electron microscopy grids coated with a perforated carbon film. After draining the excess liquid with a filter paper, grids were quickly plunged into liquid ethane and mounted onto a Gatan 626 cryoholder. Cryo-EM observation was performed with a Tecnai F20 (Fei Company) microscope operated at 200 kV, and images were recorded with a USC1000-SSCCD camera (Gatan).

Immunoblotting

293T cells were transfected for AAV production using scAAV-CBA-HA-*Lhfpl5*, as described above. Cells were lysed using M-PER (mammalian protein extraction reagent) (Thermo Scientific) 5 days after transfection. Cell lysates were subjected to SDS-PAGE gel electrophoresis, and proteins were subsequently transferred to a nitrocellulose membrane. For detection of the HA-tagged LHFPL5, we used a biotinylated anti-HA antibody (Biolegend, catalog number 901505) at 1:2,000 dilution, followed by streptavidin conjugated to horseradish peroxidase (GE Healthcare, 1:25,000 dilution). Specific antibody binding was detected by incubating the membrane with Pierce ECL Western Blotting Substrate (Thermo Scientific) and exposing autoradiographic film to the membrane.

Cochlear Culture

To assess viral transduction by different vectors in vitro, we explanted cochleas from CD1 wild-type mice at P1. Briefly, after dissecting out the temporal bone, we opened the bone and the cochlear coil from the

scala vestibuli side. Next, we removed the stria vascularis and detached the coil from the modiolus. The spiral ligament was kept in place to improve plating of the cochleas. The specimen was plated onto a glass-bottom dish (P35G-1.5-14-C; Mattek) using a tissue glue (Cell-Tak, Corning). Cochleas were cultured in DMEM supplemented with 5% fetal bovine serum, 1% N2 supplement (Thermo-Fischer), and 5 μg/mL carbenicillin. After overnight culture, we added the vector solution in 200 μL of medium at a dose of 10^{11} GCs per cochlea (unless indicated otherwise). After overnight incubation, we changed the media and kept the cochleas in culture for 3 more days to the equivalent of P6.

Cochlear Immunostaining and Imaging

Cochleas were fixed with 4% formaldehyde in PBS for 20 min. Fixed cochleas were washed three times with PBS to remove fixative and were blocked with 5% normal goat serum and permeabilized with 0.3% Triton X-100 in PBS for 1 hr at 22°C. Primary antibodies were diluted in 5% normal goat serum (NGS)/0.1% Triton X-100/PBS and incubated overnight at 4°C. To stain hair cells, we used rabbit polyclonal anti-myosin VIIa antibody (Proteus Biosciences, 1:500 dilution) with a goat anti-rabbit immunoglobulin G (IgG) secondary antibody conjugated to Alexa Fluor 647 in a 1:1,000 dilution for 1 hr (Life Technologies). To stain the hair bundle actin, we used phalloidin conjugated to Alexa Fluor 544 (Life Technologies) (1:100). To stain for the HA tag, we used an anti-HA antibody (C29F4, rabbit; Cell Signaling Technology). GFP was detected with its intrinsic fluorescence. Tissues were mounted on a Colorfrost glass slide (Thermo-Fischer Scientific) using Prolong Gold Antifade mounting medium (Thermo-Fischer). Imaging was performed with an Olympus FluoView 1000 confocal microscope (Olympus) using a PlanApoN 60×/1.42NA oil-immersion objective.

FM1-43 Loading

We assessed the ability of hair cells to accumulate the styryl dye FM1-43 to test functional restoration of hair cell mechanotransduction in culture. Cultured cochleas were quickly washed twice with Leibovitz's L15 medium (GIBCO) and incubated in the presence of 2 μM FM1-43 dye (Thermo-Fisher) for 30 s. Excess dye was removed by chelation using 0.2 mM SCAS (4-sulfonato calix[8]arene, sodium salt, from Biotium) for 2 min. Imaging was performed with an upright Olympus FluoView 1000 confocal microscope (Olympus) using a LUMPLanFI/IR 60×/1.1 water-dipping objective.

In Vivo Cochlear Injections

For in vivo analysis, we performed procedures on P0 or P1 wild-type mouse pups of the CD1 strain. After injection, we waited 14 days before sacrifice to assess vector transduction.

Cochleostomy

P0 to P1 CD1 pups were anesthetized by hypothermia, and then kept on an ice pack during the procedure. A small incision was made underneath the external ear. The incision was enlarged, and soft tissues were pushed apart using an eyelid retractor to expose the bulla. The bulla was then opened, following the stapedial artery, using a 25-μm flattened microprobe. Soft connective tissues were removed to get access to the lateral wall of the cochlea. A glass pipette was inserted through the lateral wall perpendicular to the stria vascularis to a depth of 300 μm, then 250 nL of solution (containing 5×10^9 GCs of AAV) was injected at a constant rate of 45 nL/min using a Nanoliter 2000 Injector (World Precision Instruments). We closed surgical incisions with two to three sutures using a 7-0 Vycril surgical suture. Following surgery, the pups were maintained at 37°C until complete recovery (10–15 min).

Round Window Membrane Injection

As for cochleostomy, the bulla was exposed and opened. Then, the round window niche was localized visually. Covering connective tissues were removed in order to expose the round window. We injected 250 nL of vector solution at a rate of 45 nL/min for adequate comparison with cochleostomy (introducing 5×10^9 GCs of AAV for GFP expression experiments). For rescue experiments, we injected 1–1.2 μL of the exo-AAV1-HA-*Lhfpl5* construct into the ear (2.7×10^9 GCs). We closed surgical incisions with two to three sutures using a 7-0 Vycril surgical suture.

Image Analysis

To compare transduction efficiency between conventional AAV and exo-AAV, we determined the percentage of GFP-positive hair cells and the intensity of GFP expression. To determine the percentage of GFP-positive cells, we manually counted GFP-positive and GFP-negative cells in in vitro cultures for three regions in each cochlea (approximately 120 hair cells/image). For in vivo injections, we captured eight high-magnification images along the cochlea at exactly the same distance from the base for all cochleas. Then, in each case, an investigator blinded to the vector used counted all visible hair cells on four of the images (always using the locations) and determined the percentage of GFP-positive cells. For intensity determination, we used Imaris 8.1 software (Bitplane AG). Briefly, we segmented individual hair cells based on myosin VIIa fluorescence and quantified GFP fluorescence in IHCs and OHCs separately. Measurements were normalized to the GFP intensity values from hair cells in non-injected cochleas, which were segmented the same way. We only counted GFP-positive hair cells (scored as having a GFP intensity 2 SDs above the mean background) to avoid transduction rate as a confounding variable. To quantify FM1-43 fluorescence intensity on *z*-stacks of images, we used ImageJ 1.46r software. When comparing different groups, we always used the same imaging settings, including zoom settings, pixel ratio, and *z*-step size.

Auditory Brainstem Response

The ABR assay was performed using a Tucker Davis Technologies workstation (System III; TDT). Mice were anesthetized by intraperitoneal injection of a ketamine (100 mg/kg)/xylazine (10 mg/kg) cocktail. Anesthetized mice were then placed on a heating pad, and electrodes were placed subcutaneously in the vertex, underneath the left or right ear, and on the back near the tail. Tone stimuli of 4, 5.6, 8, 11.2, 16, 22, 32, and 45.3 kHz were calibrated with a precision microphone system (PS9200 Kit; ACO Pacific) using the TDT SigCal

software package. The recorded signals were band-pass filtered (300 Hz to 3 kHz) and amplified 100,000 times. The number of acquisition trials was set to 500 averages. Maximum stimulus intensity was set to a 95-dB peak SPL, with attenuation decreasing from 85 dB to 0 dB SPL at 5-dB intervals. Band-pass filters (500–3,000 Hz) were applied to the traces before analysis.

Behavioral Tests

Startle Response

A simple startle response was performed. Briefly, animals were placed in an opaque white bucket and allowed to equilibrate for several minutes in quiet. An investigator performed a hand clap, which was not visible to the animals. The animals were filmed by a Panasonic HCV550 camera at the age of 4 weeks. *Lhfpl5* knockout animals never responded.

Open Field Test and Behavioral Function Quantification

We used a 37-cm-diameter arena with low and even illumination. Animals were tested at the age of 6 weeks. Animals were placed on the side of the arena and were filmed for 5 min. After each mouse, the arena was cleaned to avoid olfactory distractions. To quantify head tossing and circling, videos were analyzed by two investigators who were blinded to the genotype or the injection status of the animals. For head tossing, 3 separate min were counted and averaged for each investigator. The average scores assigned by each separate investigator showed a strong positive correlation (Spearman $r = 0.86$, $p = 1.76 \times 10^{-11}$). Circling was quantified using the Ethovision XT software package (Noldus). We counted full circle rotations during a 5-min observation period (360° turns in either the clockwise or counterclockwise direction).

Head tossing and circling behavior were tested at 2 separate days. The results between the 2 days showed a strong correlation (Spearman test, for head tossing: rho = 0.7, $p < 0.05$; for circling: rho = 0.85, $p < 0.001$).

Statistics

To compare two non-related sample groups, we used a t test for two independent samples or a Mann-Whitney U test. For normality testing, we used the Shapiro-Wilk test. For correlations, we used Spearman correlation. To test the relationship between the location on the cochlea and virus transduction, we performed the repeated-measures ANOVA test. For statistical testing, we used the GraphPad Prism software. $p < 0.05$ was considered statistically significant.

SUPPLEMENTAL INFORMATION

Supplemental Information includes eight figures and two movies and can be found with this article online at http://dx.doi.org/10.1016/j.ymthe.2016.12.010.

AUTHOR CONTRIBUTIONS

B.G., C.A.M., and D.P.C. conceived the study. B.G., C.S., D.I.S., A.A.I., A.R.B., S.T., D.M., Z.F., P.I.T., Y.L., A.V., X.W., and M.E. designed, performed, and analyzed experiments. C.A.M., D.P.C., and X.O.B. supervised the work. C.A.M., X.O.B., D.P.C., and A.R.B. provided support for the study. B.G., C.A.M., and D.P.C. wrote the manuscript with participation from all authors. B.G. and C.S. contributed equally to the work.

CONFLICTS OF INTEREST

C.A.M. has a patent application related to the exo-AAV (vexosome) technology and has received royalty payments from agreements between Partners Healthcare and Exosome Diagnostics, Inc. C.A.M., B.G., and D.P.C. have submitted a patent application related to cochlear gene transfer with exo-AAV.

ACKNOWLEDGMENTS

This work was supported by NIH/NINDS grant R21 NS081374-01 (C.A.M.), NIH/NIDCD grant R01 DC002281 (D.P.C.), an American Brain Tumor Association Discovery grant (C.A.M.), and a Cure Alzheimer's Fund (C.A.M.). We acknowledge the Nucleic Acid Quantitation Core at MGH Neuroscience Center for quantitative PCR analysis. B.G. is an Associate and D.P.C. is an Investigator of the Howard Hughes Medical Institute. We thank Hunter Elliott (Harvard, Image and Data Analysis Core) for assistance with image analysis. We also thank Nick Andrews and Trishala Chari (Boston Children's Hospital, Neurodevelopmental Behavioral Core) for helping with behavioral analysis.

REFERENCES

1. Lin, F.R., Niparko, J.K., and Ferrucci, L. (2011). Hearing loss prevalence in the United States. Arch. Intern. Med. *171*, 1851–1852.
2. Alzheimer's Association (2016). 2016 Alzheimer's disease facts and figures. Alzheimers Dement. *12*, 459–509.
3. Mason, J.A., and Herrmann, K.R. (1998). Universal infant hearing screening by automated auditory brainstem response measurement. Pediatrics *101*, 221–228.
4. Géléoc, G.S., and Holt, J.R. (2014). Sound strategies for hearing restoration. Science *344*, 1241062.
5. Wise, A.K., Tu, T., Atkinson, P.J., Flynn, B.O., Sgro, B.E., Hume, C., O'Leary, S.J., Shepherd, R.K., and Richardson, R.T. (2011). The effect of deafness duration on neurotrophin gene therapy for spiral ganglion neuron protection. Hear. Res. *278*, 69–76.
6. Kawamoto, K., Sha, S.H., Minoda, R., Izumikawa, M., Kuriyama, H., Schacht, J., and Raphael, Y. (2004). Antioxidant gene therapy can protect hearing and hair cells from ototoxicity. Mol. Ther. *9*, 173–181.
7. Kawamoto, K., Yagi, M., Stöver, T., Kanzaki, S., and Raphael, Y. (2003). Hearing and hair cells are protected by adenoviral gene therapy with TGF-beta1 and GDNF. Mol. Ther. *7*, 484–492.
8. Li, W., Wu, J., Yang, J., Sun, S., Chai, R., Chen, Z.Y., and Li, H. (2015). Notch inhibition induces mitotically generated hair cells in mammalian cochleae via activating the Wnt pathway. Proc. Natl. Acad. Sci. USA *112*, 166–171.
9. Liberman, M.C., Gao, J., He, D.Z., Wu, X., Jia, S., and Zuo, J. (2002). Prestin is required for electromotility of the outer hair cell and for the cochlear amplifier. Nature *419*, 300–304.
10. Kohrman, D.C., and Raphael, Y. (2013). Gene therapy for deafness. Gene Ther. *20*, 1119–1123.
11. Sacheli, R., Delacroix, L., Vandenackerveken, P., Nguyen, L., and Malgrange, B. (2013). Gene transfer in inner ear cells: a challenging race. Gene Ther. *20*, 237–247.
12. Akil, O., Seal, R.P., Burke, K., Wang, C., Alemi, A., During, M., Edwards, R.H., and Lustig, L.R. (2012). Restoration of hearing in the VGLUT3 knockout mouse using virally mediated gene therapy. Neuron *75*, 283–293.

13. Askew, C., Rochat, C., Pan, B., Asai, Y., Ahmed, H., Child, E., Schneider, B.L., Aebischer, P., and Holt, J.R. (2015). Tmc gene therapy restores auditory function in deaf mice. Sci. Transl. Med. *7*, 295ra108.

14. Fitzpatrick, Z., György, B., Skog, J., and Maguire, C.A. (2014). Extracellular vesicles as enhancers of virus vector-mediated gene delivery. Hum. Gene Ther. *25*, 785–786.

15. György, B., Hung, M.E., Breakefield, X.O., and Leonard, J.N. (2015). Therapeutic applications of extracellular vesicles: clinical promise and open questions. Annu. Rev. Pharmacol. Toxicol. *55*, 439–464.

16. György, B., Fitzpatrick, Z., Crommentuijn, M.H., Mu, D., and Maguire, C.A. (2014). Naturally enveloped AAV vectors for shielding neutralizing antibodies and robust gene delivery in vivo. Biomaterials *35*, 7598–7609.

17. Maguire, C.A., Balaj, L., Sivaraman, S., Crommentuijn, M.H., Ericsson, M., Mincheva-Nilsson, L., Baranov, V., Gianni, D., Tannous, B.A., Sena-Esteves, M., et al. (2012). Microvesicle-associated AAV vector as a novel gene delivery system. Mol. Ther. *20*, 960–971.

18. Xiong, W., Grillet, N., Elledge, H.M., Wagner, T.F., Zhao, B., Johnson, K.R., Kazmierczak, P., and Müller, U. (2012). TMHS is an integral component of the mechanotransduction machinery of cochlear hair cells. Cell *151*, 1283–1295.

19. Hudry, E., Martin, C., Gandhi, S., György, B., Scheffer, D.I., Mu, D., Merkel, S.F., Mingozzi, F., Fitzpatrick, Z., Dimant, H., et al. (2016). Exosome-associated AAV vector as a robust and convenient neuroscience tool. Gene Ther. *23*, 380–392.

20. Gibson, F., Walsh, J., Mburu, P., Varela, A., Brown, K.A., Antonio, M., Beisel, K.W., Steel, K.P., and Brown, S.D. (1995). A type VII myosin encoded by the mouse deafness gene shaker-1. Nature *374*, 62–64.

21. Anderson, D.W., Probst, F.J., Belyantseva, I.A., Fridell, R.A., Beyer, L., Martin, D.M., Wu, D., Kachar, B., Friedman, T.B., Raphael, Y., et al. (2000). The motor and tail regions of myosin XV are critical for normal structure and function of auditory and vestibular hair cells. Hum. Mol. Genet. *9*, 1729–1738.

22. Di Palma, F., Holme, R.H., Bryda, E.C., Belyantseva, I.A., Pellegrino, R., Kachar, B., Steel, K.P., and Noben-Trauth, K. (2001). Mutations in Cdh23, encoding a new type of cadherin, cause stereocilia disorganization in waltzer, the mouse model for Usher syndrome type 1D. Nat. Genet. *27*, 103–107.

23. Yu, Q., Wang, Y., Chang, Q., Wang, J., Gong, S., Li, H., and Lin, X. (2014). Virally expressed connexin26 restores gap junction function in the cochlea of conditional Gjb2 knockout mice. Gene Ther. *21*, 71–80.

24. Longo-Guess, C.M., Gagnon, L.H., Cook, S.A., Wu, J., Zheng, Q.Y., and Johnson, K.R. (2005). A missense mutation in the previously undescribed gene Tmhs underlies deafness in hurry-scurry (hscy) mice. Proc. Natl. Acad. Sci. USA *102*, 7894–7899.

25. McCarty, D.M., Monahan, P.E., and Samulski, R.J. (2001). Self-complementary recombinant adeno-associated virus (scAAV) vectors promote efficient transduction independently of DNA synthesis. Gene Ther. *8*, 1248–1254.

26. Wang, Z., Ma, H.I., Li, J., Sun, L., Zhang, J., and Xiao, X. (2003). Rapid and highly efficient transduction by double-stranded adeno-associated virus vectors in vitro and in vivo. Gene Ther. *10*, 2105–2111.

27. Xiao, X., Li, J., and Samulski, R.J. (1998). Production of high-titer recombinant adeno-associated virus vectors in the absence of helper adenovirus. J. Virol. *72*, 2224–2232.

28. Rabinowitz, J.E., Rolling, F., Li, C., Conrath, H., Xiao, W., Xiao, X., and Samulski, R.J. (2002). Cross-packaging of a single adeno-associated virus (AAV) type 2 vector genome into multiple AAV serotypes enables transduction with broad specificity. J. Virol. *76*, 791–801.

YMTHE, Volume *25*

Supplemental Information

Rescue of Hearing by Gene Delivery to Inner-Ear Hair Cells Using Exosome-Associated AAV

Bence György, Cyrille Sage, Artur A. Indzhykulian, Deborah I. Scheffer, Alain R. Brisson, Sisareuth Tan, Xudong Wu, Adrienn Volak, Dakai Mu, Panos I. Tamvakologos, Yaqiao Li, Zachary Fitzpatrick, Maria Ericsson, Xandra O. Breakefield, David P. Corey, and Casey A. Maguire

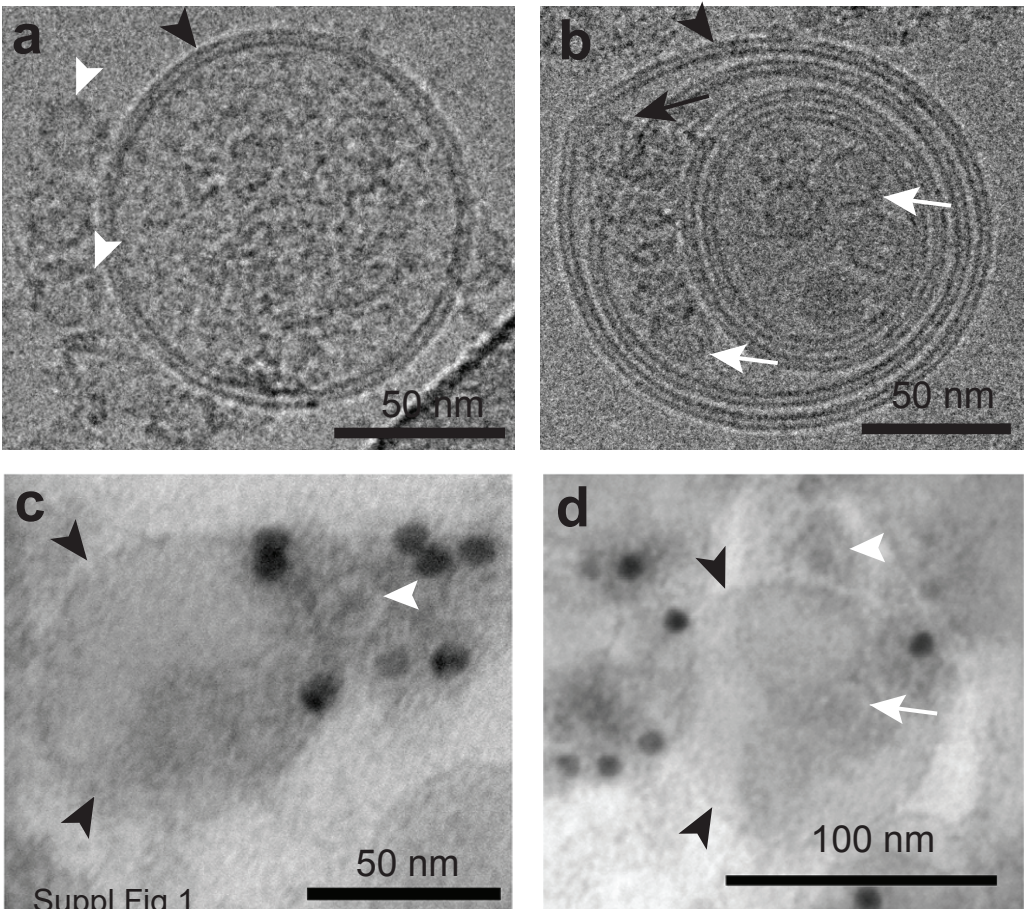

Suppl Fig 1

Suppl. Fig 2

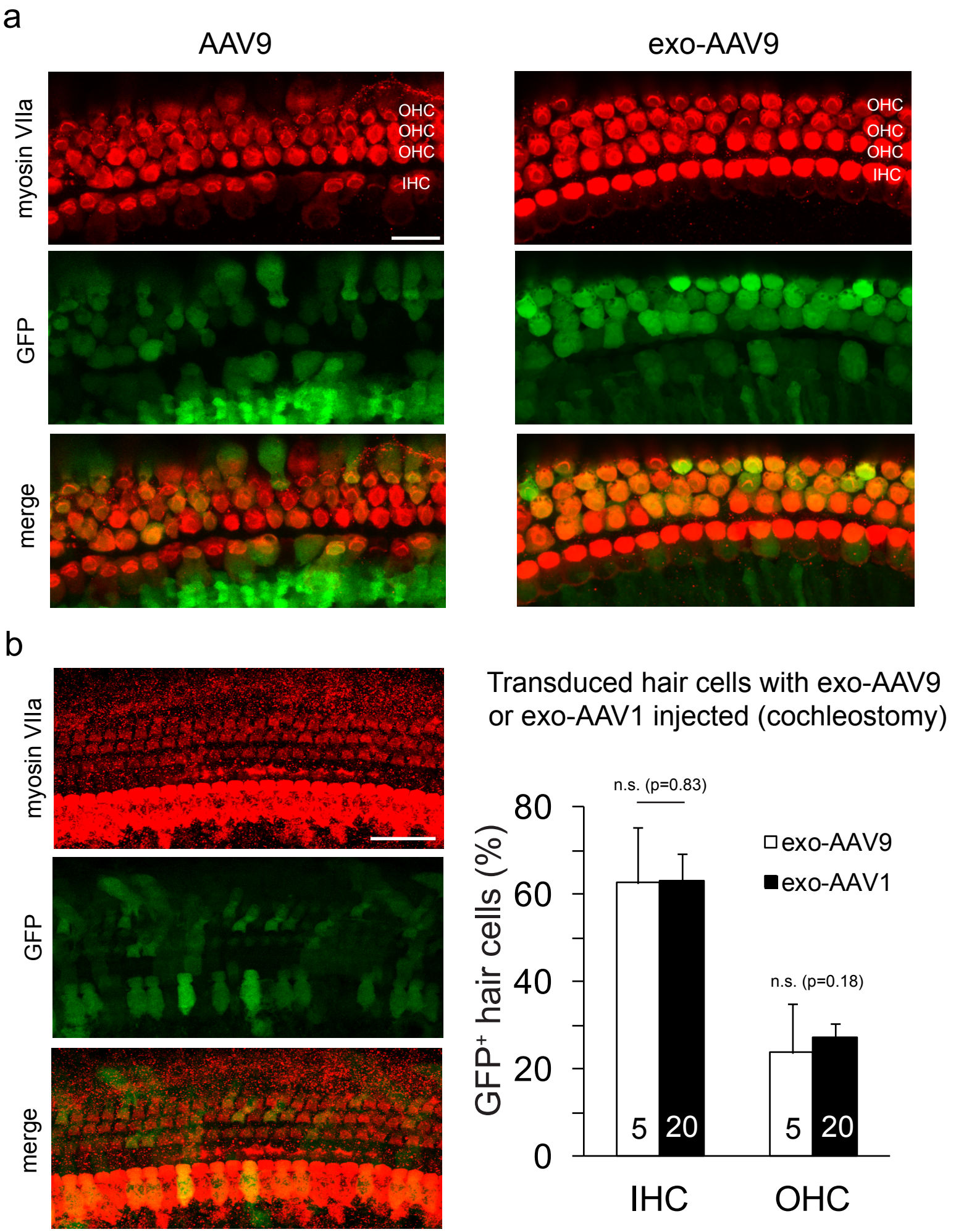
a
AAV9
exo-AAV9
myosin VIIa
GFP
merge
OHC
OHC
OHC
IHC
b
Transduced hair cells with exo-AAV9
or exo-AAV1 injected (cochleostomy)
n.s. (p=0.83)
n.s. (p=0.18)
GFP+ hair cells (%)
80
60
40
20
0
exo-AAV9
exo-AAV1
5
20
5
20
IHC
OHC

Suppl. Fig. 3

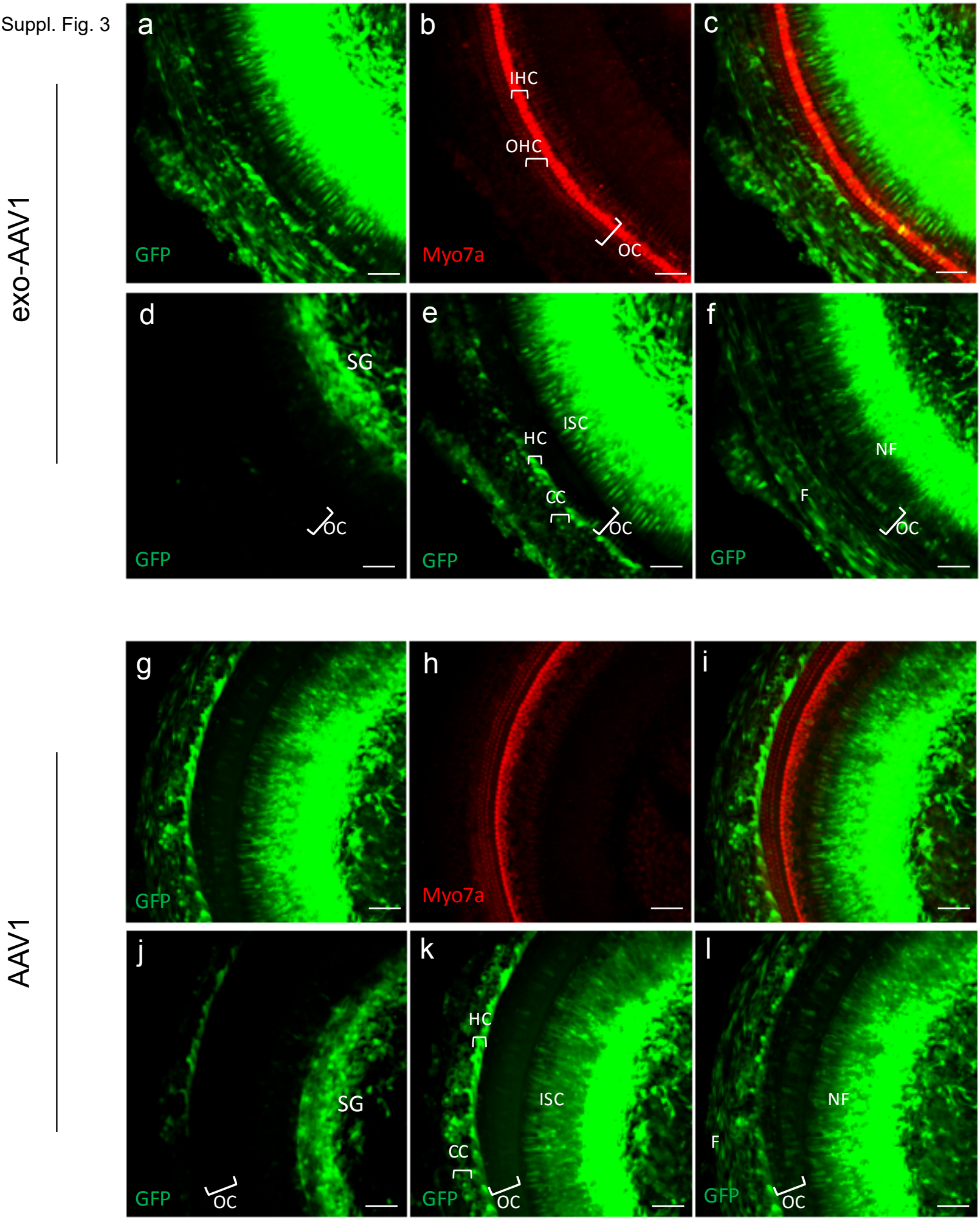
exo-AAV1
AAV1
a
b
c
d
e
f
g
h
i
j
k
l
GFP
Myo7a
IHC
OHC
OC
SG
HC
ISC
CC
NF
F

Suppl Fig 4.

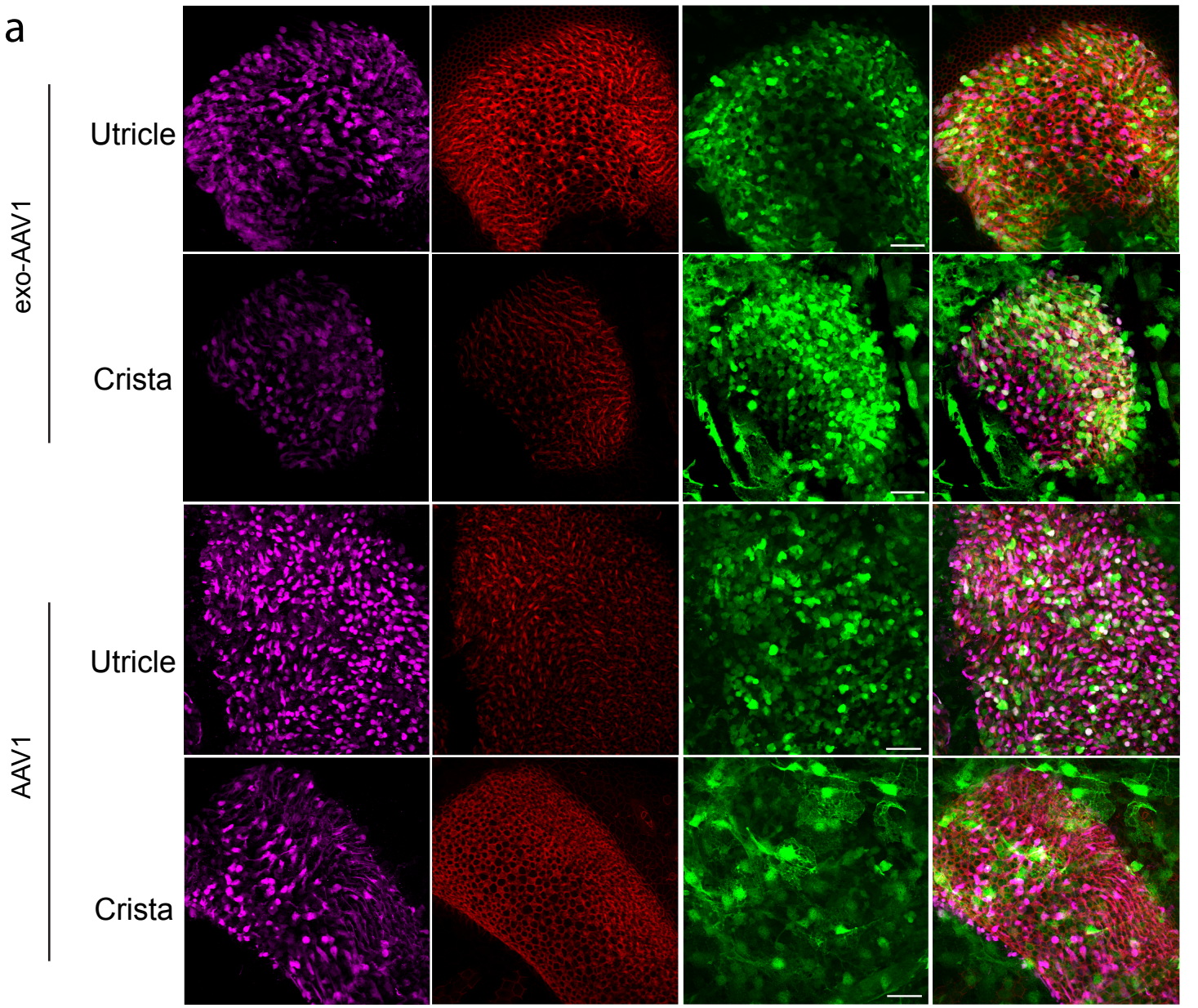
a
exo-AAV1
Utricle
Crista
AAV1
Utricle
Crista

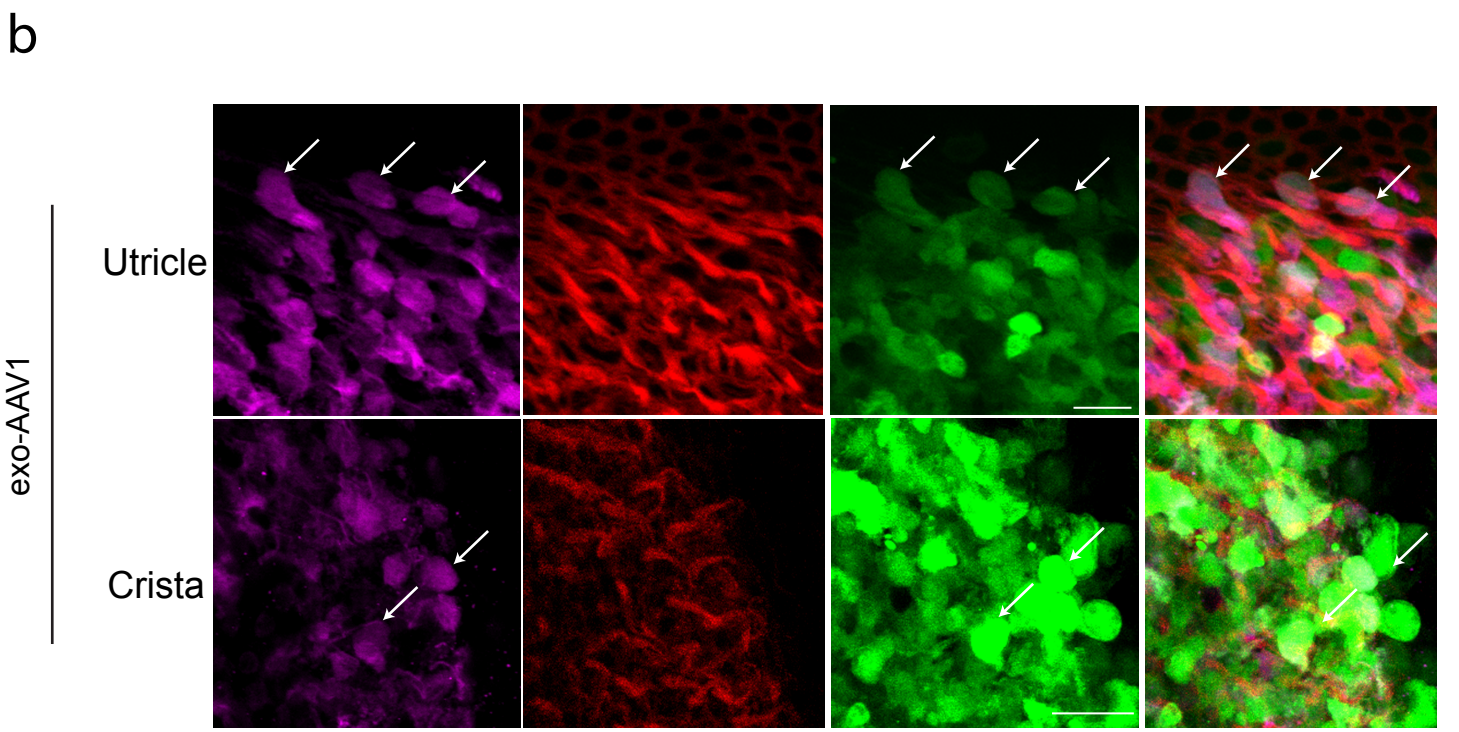
b
exo-AAV1
Utricle
Crista

Suppl. Fig. 5

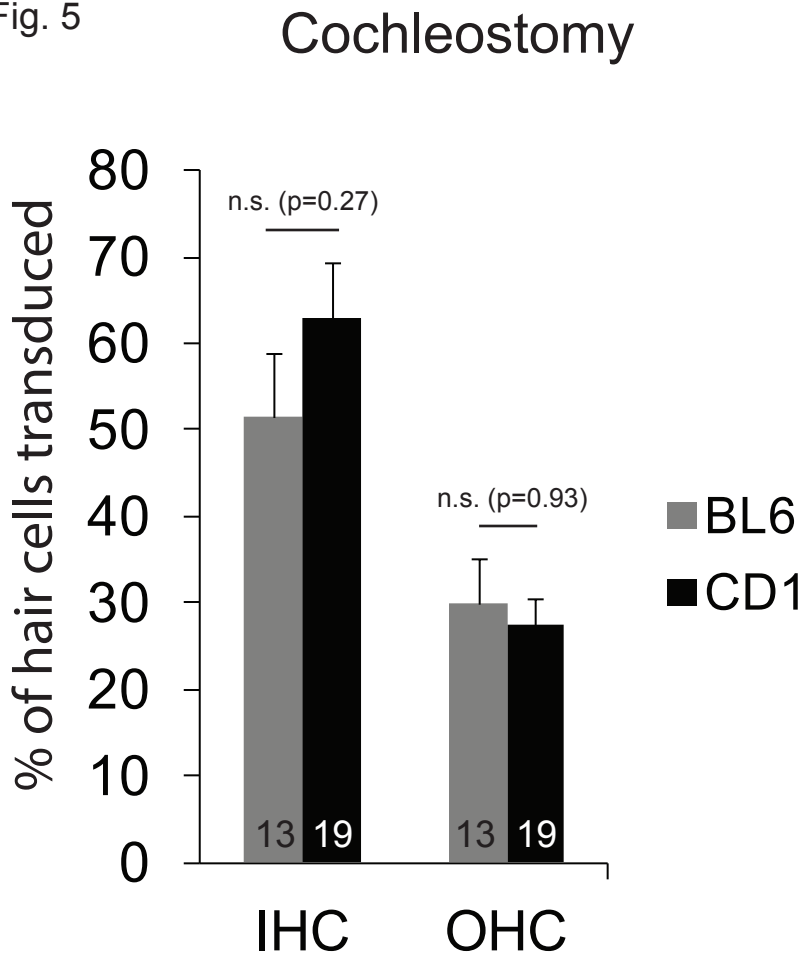
Cochleostomy
% of hair cells transduced
80
70
60
50
40
30
20
10
0
n.s. (p=0.27)
n.s. (p=0.93)
13
19
13
19
IHC
OHC
BL6
CD1

Suppl Fig. 6

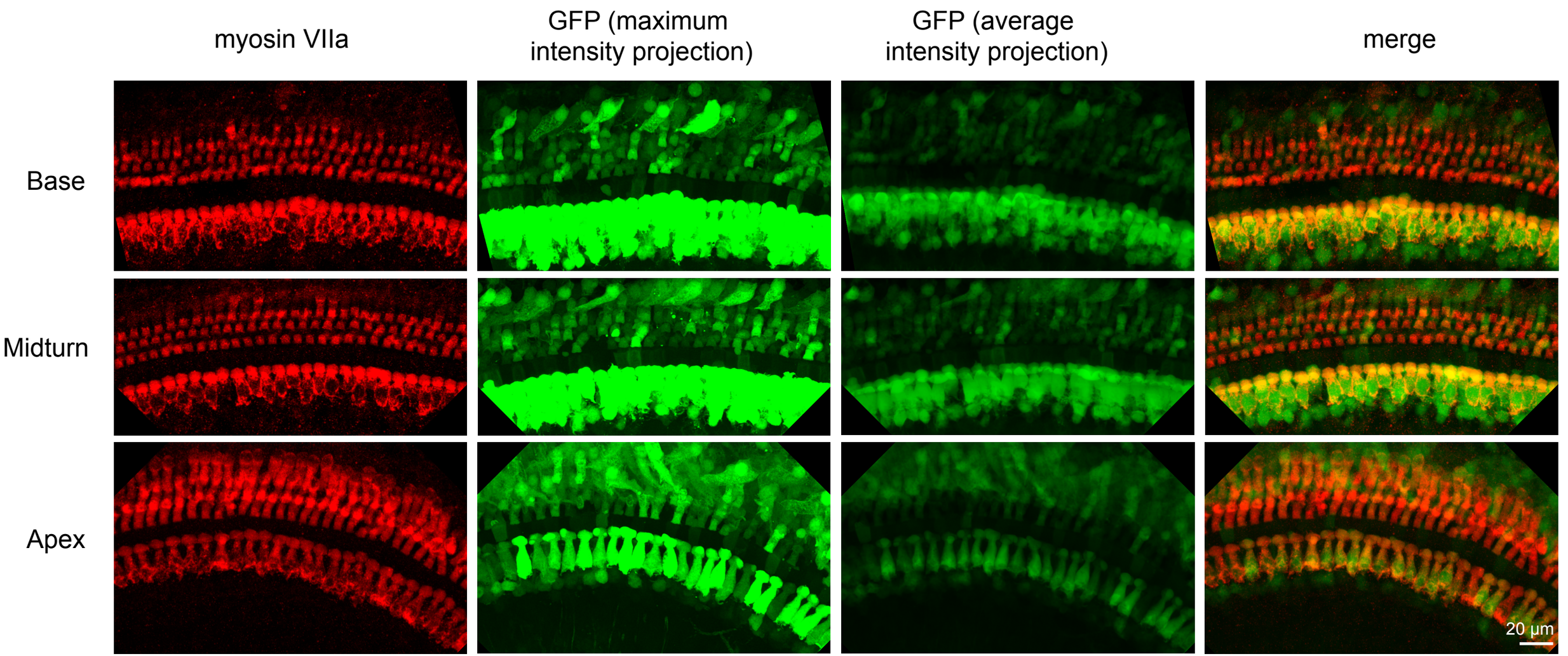
myosin VIIa
GFP (maximum intensity projection)
GFP (average intensity projection)
merge
Base
Midturn
Apex
20 µm

Suppl Fig. 7

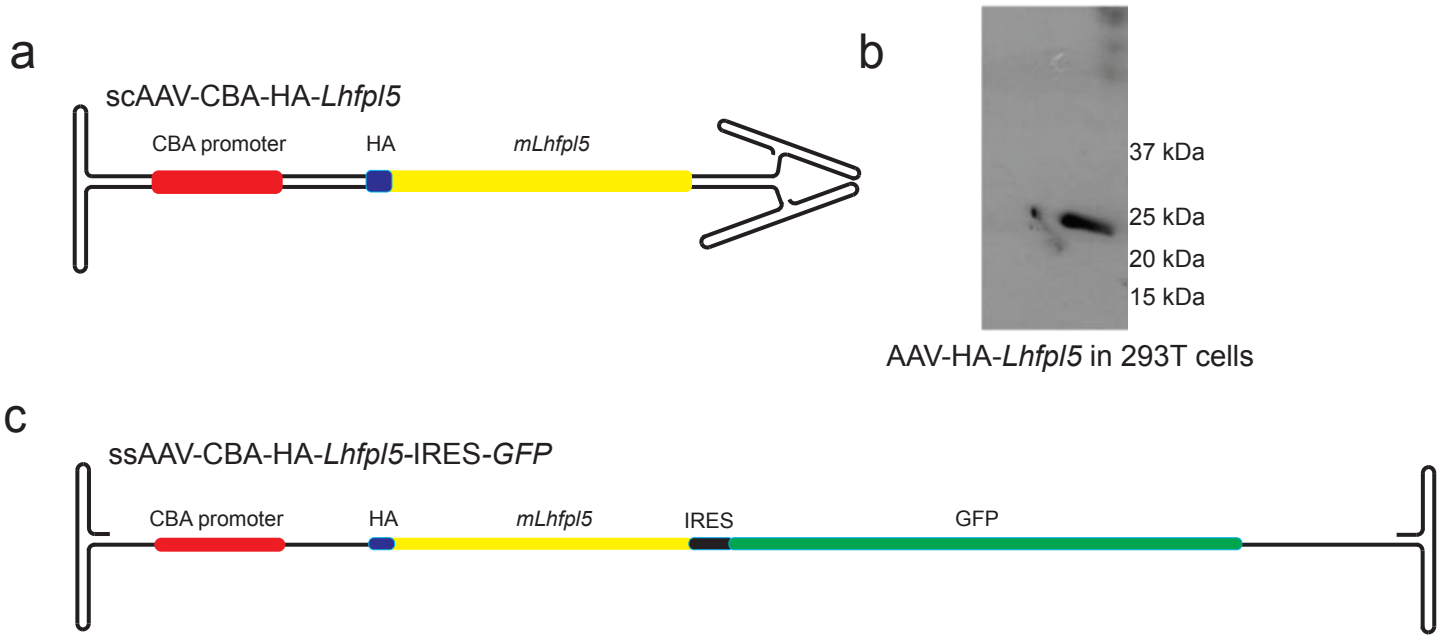
a
scAAV-CBA-HA-*Lhfpl5*
CBA promoter
HA
mLhfpl5
b
37 kDa
25 kDa
20 kDa
15 kDa
AAV-HA-*Lhfpl5* in 293T cells
c
ssAAV-CBA-HA-*Lhfpl5*-IRES-*GFP*
CBA promoter
HA
mLhfpl5
IRES
GFP

Suppl. Fig. 8

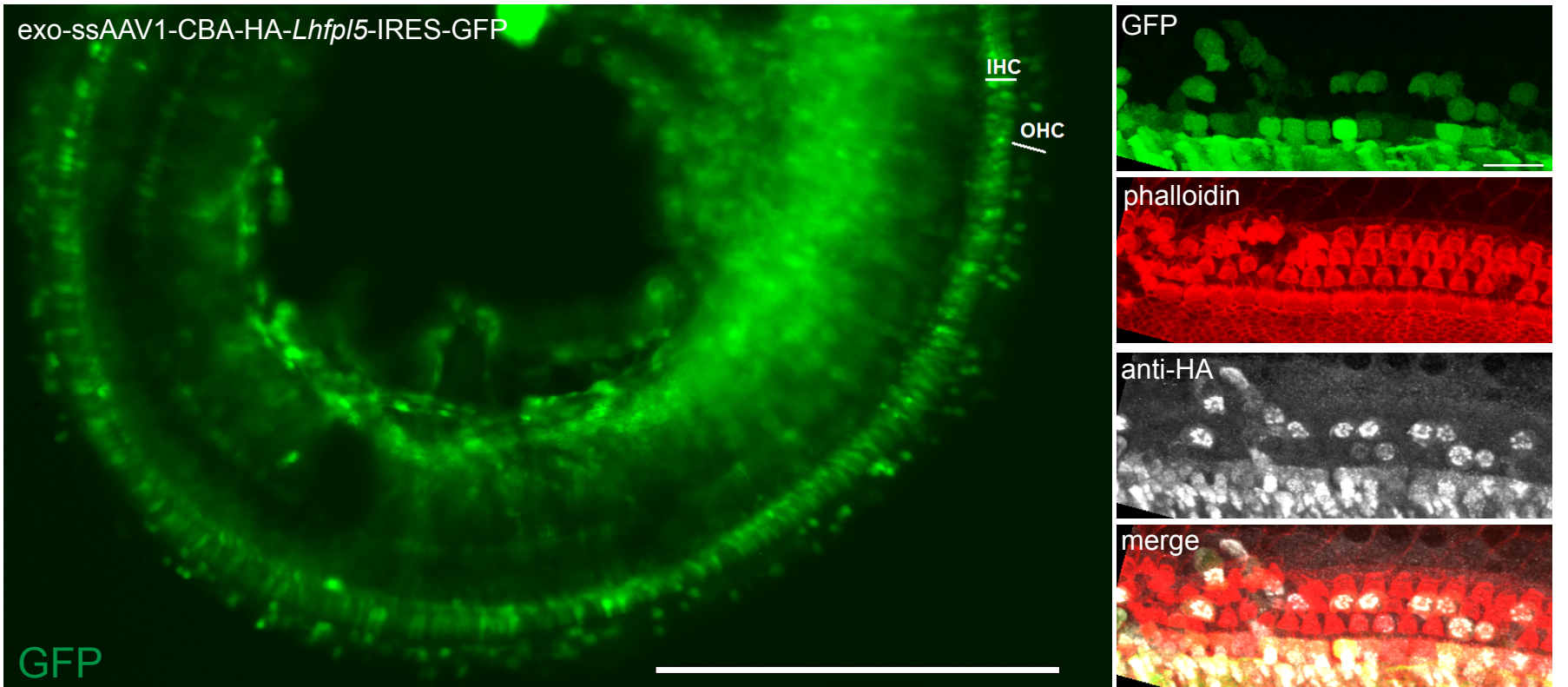
exo-ssAAV1-CBA-HA-*Lhfpl5*-IRES-GFP
IHC
OHC
GFP
GFP
phalloidin
anti-HA
merge

Supplementary Figures and Videos

Supplementary Figure 1. **AAV1 associates with exosomes**. **(a,b)** Cryo-electron microscopy images showing AAV on the surface (a) or the interior (b) of exosomes. Black arrowheads point to exosomal membrane; white arrowheads show AAV capsids on the exterior of the vesicle; white arrows show capsids that appear to be on the interior of the exosome; and black arrow shows one AAV capsid distorting the membrane suggesting it is on the interior of the vesicle. Scale bars are 50 nm. **(c, d)** Transmission electron micrographs of cryosectioned exo-AAV samples that were immunogold-labeled to detect intact AAV1 capsids. AAV capsids are seen on the surface (white arrowheads, c and d) or inside exosomes (white arrow, d). Black arrowheads indicate exosome membrane. Scale bars are 50 nm (c) or 100 nm (d).

Supplementary Figure 2. Exo-AAV9-CBA-GFP outperforms conventional AAV9-CBA-GFP in transduction of cochlear explant hair cells. (a) *In vitro*. Cochleas were explanted from CD1 mice at P1. Vectors were added at $1x10^{11}$ GC the next day for overnight transduction and organs were cultured for three more days. Exo-AAV9-GFP efficiently transduces IHCs and OHCs, labeled with anti-myosin VIIa antibody. Viral transduction is quantified in Fig. 1e. Scale bar is 20 μm. **(b)** *In vivo.* Exo-AAV9 was injected by cochleostomy. The number of hair cells transduced with exo-AAV9 *in vivo* was similar that transduced with exo-AAV1. Scale bar is 30 μm. *Right*, there was no difference between exo-AAV1 and exo-AAV9 in vivo. Exo-AAV1 values are replotted from Fig. 2b for reference. Mean ± SEM.

Supplementary Figure 3. Transduction of cochlear cells by exo-AAV1-GFP and AAV1-GFP vectors administered by cochleostomy. Middle turn of a cochlea at low magnification. CD1 mice were injected at P1, then cochleas were dissected at P14. Hair cells were stained with anti-myosin VIIa antibody (red). **(a-f)** Exo-AAV1. Panels a,d,e,f are confocal images at four different depths. **(g-l)** AAV1**.** Panels g,j,k,l are confocal images at four different depths. For both, other cell types are also efficiently transduced. OC: organ of Corti, IHC: inner hair cell, OHC: outer hair cell, SG: spiral ganglia neurons, ISC: inner sulcus cells, HC: Hensen cells, CC: Claudius cells, NF: nerve fibers, F: fibroblasts. Scale bars: 60 μm.

Supplementary Figure 4. Transduction of the vestibular sensory epithelium by exo-AAV1-GFP and AAV1-GFP vectors, administered by cochleostomy. (a) Low magnification. CD1 mice were injected at P0/P1; the utricle and the ampulla of the lateral semicircular canal were dissected at P14. Hair cells were stained with antibodies to myosin VIIa (purple); actin was labeled with phalloidin (red); and GFP is green. Many vestibular hair cells and supporting cells were transduced, even though the vector was delivered to the cochlea. Scale bars are 30 μm. (b) High magnification. Images show colocalization of GFP with myosin VIIa in hair cells (arrows). Scale bars are 10 μm.

Supplementary Figure 5. Comparison of exo-AAV1-GFP transduction efficiency in CD1 and C57BL/6 mice; injection by cochleostomy. The difference between CD1 (data from Fig. 2b) and C57BL/6 was not significant for either IHCs or OHCs (Mann-Whitney U test). Mean ± SEM.

Supplementary Figure 6. Maximum observed transduction using exo-AAV1 delivered by cochleostomy. C57BL/6 mice were injected by cochleostomy using 0.3 µl of exo-AAV1-CBA-GFP at P1 (resulting in $6x10^9$ GC injected). Cochleas were dissected at P14. Images represent the cochlea with the highest number of GFP-positive hair cells (assessed with direct GFP fluorescence). Scale bar is 20 µm.

Supplementary Figure 7. Schematic of the vectors used in the study. (a) Self-complimentary (sc) AAV-*Lhfpl5* constructs. We synthesized a mouse codon-optimized AAV expression cassette containing a hemagglutinin (HA) tag on the N-terminus. Expression was driven by the chicken beta-actin (CBA) promoter. **(b)** Western blot of protein from AAV-producer 293T cells using anti-HA. LHFPL5 protein has a molecular weight of 24 kDa. **(c)** Schematic of the single stranded (ss) AAV-CBA-*HA-Lhfpl5*-IRES-*GFP* construct. IRES: internal ribosomal entry site.

Supplementary Figure 8. Co-expression of GFP and HA-LHFPL5 after i*n vivo* injection of exo-AAV-CBA-*HA-Lhfpl5*-IRES-*GFP*. *Lhfpl5*$^{-/-}$ mice (C57BL/6 background) were injected through the round window at P1 and cochleas were dissected at P6. The single-stranded construct transduced IHCs and OHCs, revealed by GFP expression. Furthermore, GFP-positive cells showed anti-HA labeling in the cell body and in the bundle, confirming the correlation between GFP expression and LHFPL5 localization in bundles. Scale bars are 400 µm (left panel) and 20 µm (right panel).

Supplementary Video 1. Startle response. *Lhfpl5*$^{+/-}$, *Lhfpl5*$^{-/-}$, and *Lhfpl5*$^{-/-}$ animals injected with exo-AAV1-CBA-*Lhfpl5* were placed in an opaque white bucket and allowed to equilibrate for several minutes in quiet. An investigator performed a hand clap, which was not visible to the animals. Animals that can hear the clap momentarily freeze (Preyer reflex).

Supplementary Video 2. Open field test. *Lhfpl5*$^{+/-}$, *Lhfpl5*$^{-/-}$, and *Lhfpl5*$^{-/-}$ animals injected with exo-AAV1-CBA-*Lhfpl5* were placed in an opaque white arena. Normal mice explore the new environment and show head and gait stability. *Lhfpl5*$^{-/-}$ animals show head tossing, gait instability, circling and backward movement.